# Investigation into the kinetics, mechanisms and particle characteristics of selenium precipitation from copper sulphate solution

by

Murehwa Mangere

Thesis presented for the degree of

*Master of Science in Engineering*

in the Department of Chemical Engineering,

University of Cape Town

April 2010

*"Thank you Lord for lighting my path"*

This work is dedicated to my family and friends

*"I know the meaning of plagiarism and declare that all the work in the document, save for that which is properly acknowledged, is my own"*

**Acknowledgements**

I express my sincere gratitude to my project supervisor, Professor A. E. Lewis and co-supervisor, J. Nathoo for their inspired supervision and guidance in the project, a big thank you.

To the members of the Crystallization Precipitation Unit, you rock! Thank you to Christine for always being cheerful! CPU has been great fun.

I also would like to thank everyone involved in my project, directly or indirectly, special mention to Riana at Stellenbosch for her assistance with analysis of selenium and the members of the Chemistry Department, especially Prof. K. Naidoo and Dr. G. Venter for their assistance in molecular modeling.

I also thank Anglo Platinum, Les Bryson and the Crystallization and Precipitation Unit for financial support.

Most importantly, to my wife Ntando and son Munashe, thank you so much for the emotional and moral support you gave me throughout the project.

Last but not least, my parents and other family members for the patience and understanding.

**Abstract**

The removal of selenium from copper sulphate solution prior to the electrowinning of copper is desirable in order to minimise contamination of the copper cathodes by selenium and other impurities. The selenium removal is effected by a precipitation process that takes place under high supersaturation conditions which favour nucleation over any other particle formation processes. There is currently no fundamental information on the nucleation kinetics of this important process. Furthermore, the fundamental chemistry and mechanisms involved in this process are not fully understood. In this study, the nucleation kinetics, the process chemistry and mechanisms of selenium precipitation from acidic copper sulphate solution were investigated.

Nucleation kinetic experiments were carried out by varying the levels of supersaturation from $8.66 \times 10^{15}$ to $4.33 \times 10^{17}$ at a temperature of 95°C under atmospheric pressure. The nucleation rates for four different levels of supersaturation, the nucleation work and the nucleus size were determined. The kinetic constant $A$ was found to be $3.92 \times 10^{27}$ $m^{-3}s^{-1}$ and this shows that the nucleation process takes place through a homogeneous mechanism. The associated thermodynamic parameter ($B$) was determined to be $8.98 \times 10^{04}$.

Thermodynamic analysis showed that selenium exists as hydrogen selenate ($HSeO_4^-$) and hydrogen selenite ($HSeO_3^-$) in the acidic copper sulphate solution. The reduction reactions of these ions using sodium sulphite were predicted to go to completion, precipitating selenium as copper selenide ($Cu_2Se$) at an operating temperature range of 85°C to 100°C. Kinetic studies of selenium reduction revealed that the reduction of selenium (+4) ions is very fast (99.9% conversion achieved in less than 60 seconds). However, the reduction of selenium (+6) is very slow (only 45.7 % conversion achieved in 72 hours). During the reduction of selenium(+6), a brick red precipitate, which is a mixture of element copper and Chevreul's salt ($Cu_2SO_3.CuSO_3.2H_2O$) is also be formed.

A theoretical study was carried out to explain the differences in the reactivity of these selenium species. The results revealed that selenate has zero dipole moments and has a rigid molecular structure which makes it 'unreactive'. Activation energy calculations also showed that selenate has a higher transition state barrier (4.354 kcal/mol) as compared to

the selenite (3.054 kcal/mol). However, acidifying the solution resulted in a protonated selenate ion which significantly altered the molecular structure of the selenate ion. The results also showed that the interaction between protonated selenate and sulphite ions has a lower transition state barrier (3.914 kcal/mol) than for the free selenate system.

## Table of contents

**Table of figures**

**List of tables**

## Nomenclature

| Symbol | Definition | Units |
|---|---|---|
| A | Nucleation kinetic constant | $m^{-3}s^{-1}$ |
| *a* | Activity coefficient | - |
| *a** | Activity coefficient at equilibrium | - |
| B | Nucleation thermodynamic constant | - |
| $C_n(t)$ | Concentration of nuclei in the system | $N_p m^{-3}$ |
| e | Dielectric constant | - |
| $E_{sol}$ | Solvation energy | kcal/mol |
| $\Delta G$ | Change in Gibbs free energy | kcal/mol |
| $\partial H$ (T) | Enthalpy change | kcal/mol |
| J | Nucleation rate | $m^{-3}s^{-1}$ |
| k | Boltzmann constant | J/K |
| $K_{sp}$ | Solubility product | $mol^{-3}m^{-3}$ |
| $m^+$ | Concentration of cations | $mol/m^3$ |
| $m^-$ | Concentration of anions | $mol/m^3$ |
| *n* | Cluster size | - |
| *n** | Critical nucleus | - |
| $N_p$ | Number of super nuclei/particles in the system | - |
| $N_o$ | Number of particles initially in the solution | - |
| r | Probe radius | m |
| R | Universal gas constant | J/mol.K |
| S | Supersaturation ratio | - |
| $\partial S$ (T) | Entropy change | kcal/mol.K |
| T | Absolute temperature | °K |
| t | Time in seconds | s |
| $v^+$ | Cations | - |
| $v^-$ | Anions | - |
| V | Volume of the system | $m^3$ |
| W* | Nucleation work | kJ |
| $W_n$ | Gain in work | kJ |

| | | |
|---|---|---|
| $\mu$ | Solution chemical potential | $mol.dm^{-3}$ |
| $\mu_s$ | Solution chemical potential at equilibrium | $mol.dm^{-3}$ |
| $\Psi$ | Cluster total surface area | $m^2$ |

| **Abbreviation** | **Definition** |
|---|---|
| CPU | Crystallisation and Precipitation Unit |
| CNT | Classical Nucleation Theory |
| DLS | Dynamic Light Scattering |
| DFT | Density Functional Theory |
| EDS | Energy Dispersive Spectroscopy |
| ICP-MS | Inductively Coupled Plasma Mass Spectroscopy |
| PB | Poisson-Boltzmann |
| SEM | Scanning Electron Microscope |
| XRD | X ray Diffraction |
| ZPE | Zero Point Energy |

# 1.0 INTRODUCTION

## 1.1 Project background

Most copper ores contain selenium which also dissolves into the copper sulphate solution during pressure or atmospheric leaching of copper. In order to prepare the copper sulphate solution for the electrowinning of copper, selenium must be removed. Figure 1 shows a typical flowsheet of an electrolytic copper refinery plant with a selenium removal stage prior the electrowinning stage.

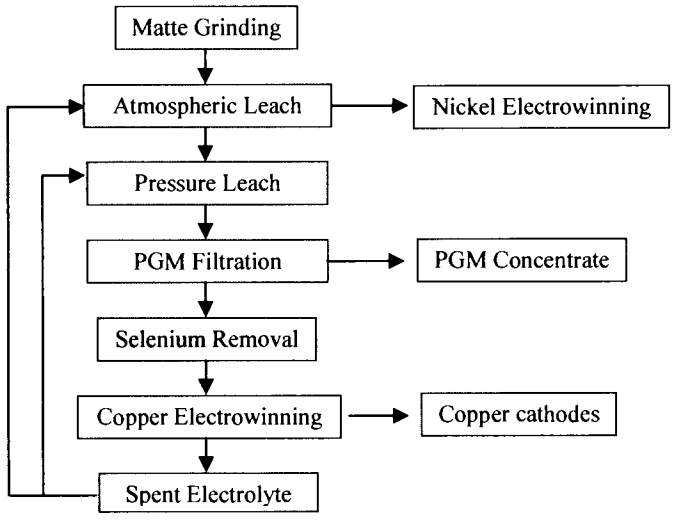


**Figure 1 – Flow sheet of a typical electrolytic refinery of copper circuit**

If selenium is not removed from the copper sulphate solution, it will co-deposit with copper on the cathode, thereby contaminating the copper product. Selenium has adverse effects on the electrical conductivity of copper and as a result contaminated copper products sell at a lower price on the metal exchange market. Therefore it is desirable to remove all the selenium from the solution before the electrowinning stage in order to get the highest premium for a quality copper product.

Selenium removal is carried out by using reductants such as sodium sulphite to precipitate out selenium as copper selenide. The reduction process is typically carried out in a pipe reactor with the subsequent aging process being done in tanks as shown in Figure 2.

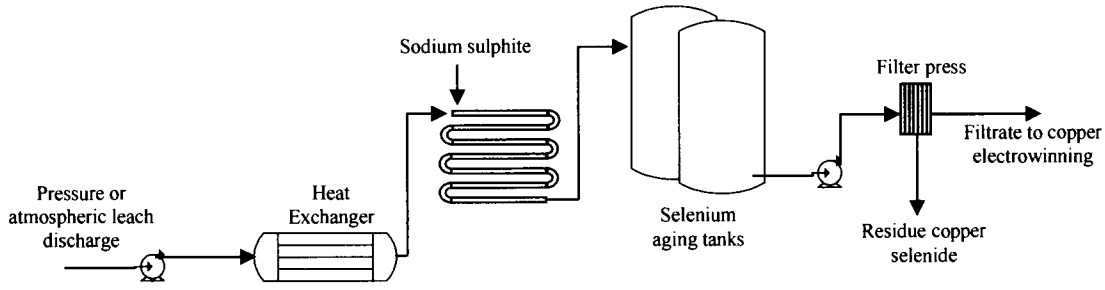


**Figure 2 – A typical selenium removal circuit**

The overall reaction for the precipitation reaction is given by equation 1.

$$H_2SeO_4 + 5Na_2SO_3 + 2CuSO_4 + H_2O = Cu_2Se + 5Na_2SO_4 + 2H_2SO_4 \qquad [1]$$

Copper selenide ($Cu_2Se$) is then filtered, and the clarified solution goes for copper electrowinning. The reduction reaction can be slow, mostly dependent on the amount of selenate ions present which are unreactive. Due to the notoriously slow reaction, the tubular reactors are usually long and include aging tanks. In many cases selenium is not completely removed from the electrowinning solution because the provided residence time is small. As a result the copper product is contaminated with selenium and results in an amorphous product structure which further entrains other impurities like lead. Therefore the development of a faster continuous selenium precipitation process will significantly improve product quality, process efficiency and plant throughput.

However, the underlying particle kinetic processes and mechanisms of this process are not fully understood. Because of a lack of fundamental understanding of the process, there are no design guidelines and thus it is potentially inefficient and uneconomical. In order to improve the current process, it is necessary to understand the particle formation kinetics, mechanisms and the reasons behind the slow reactivity of the selenium species.

## 1.2 Scope of work

Based on the above background, a study into the chemistry at molecular level and particle kinetic processes of selenium precipitation will be a significant contribution in the endeavour to develop a faster continuous process. The process of selenium precipitation from copper sulphate solution by sulphur based reductants was studied by Clark and Rickard (1975), Hofirek (1981), Nikolic and Laferty (1981) and Weir et al. (1982). These

studies focussed on the applicability of the process on an industrial scale. However, research on the fundamental particle formation processes, nucleation rates and mechanisms of the process has not been done. Therefore the main focus of this work is to determine nucleation kinetics and particle formation mechanisms of the process using the Classical Nucleation Theory (CNT).

Greater knowledge of particle formation kinetics can significantly improve the control of precipitation processes. These particle formation processes include nucleation, growth and secondary processes such as aggregation, breakage and Ostwald ripening. Nucleation kinetics play a significant role in precipitation since they are responsible for the final properties of the precipitant such as crystal size distribution and morphology. Nucleation can proceed according to two mechanisms, namely homogenous or heterogeneous. A nucleation kinetic study can yield nucleation rates, nucleation work, the nucleus size and the thermodynamic parameters that will distinguish whether nucleation takes place through homogeneous or heterogeneous mechanisms. Knowledge of these parameters is used to determine whether the process can be seeded to speed up precipitation.

In order to understand the underlying chemical kinetics, further studies were carried out prior the determination of the nucleation rate, to determine the reaction time for the selenate and selenite species. Molecular modeling was also carried out to explain the reasons for the difference in the reactivity of the different selenium species.

# 2.0 THEORY AND LITERATURE REVIEW

## 2.1 Precipitation

Precipitation is an important separation and purification technique used in many chemical industries. It can be defined as the formation of a solid product from solution as a result of the addition of a reagent to a solution. Precipitation is also called reaction crystallization. It can be classified into hydrolysis, ionic, reduction and substitution precipitation. These precipitation processes are used to separate metals, either recovering the major metal or removing impurities from solutions (Habashi, 1993; Jackson, 1986).

Precipitation occurs in thermodynamically unstable solutions in which the driving force for particle formation is the concentration of the reaction product in excess of its equilibrium value (Mullin, 1972). Hence the driving force for precipitation, also known as supersaturation, is given by the change in chemical potential between prevailing and equilibrium states. The degree of supersaturation plays a major role in the determination of the kinetics of the precipitation process. The role of supersaturation in precipitation processes can be summarized by Figure 3. It is clear that supersaturation is central to the whole outcome of precipitation. Nucleation, aging and growth kinetics influence the precipitate size distribution. The rate at which particles grow further determines the purity of the product. Transformations between various polymorphs are controlled by the transformation kinetics and the position of the system in the appropriate phase diagram also depends on the supersaturation level (Sohnel and Garside, 1992).

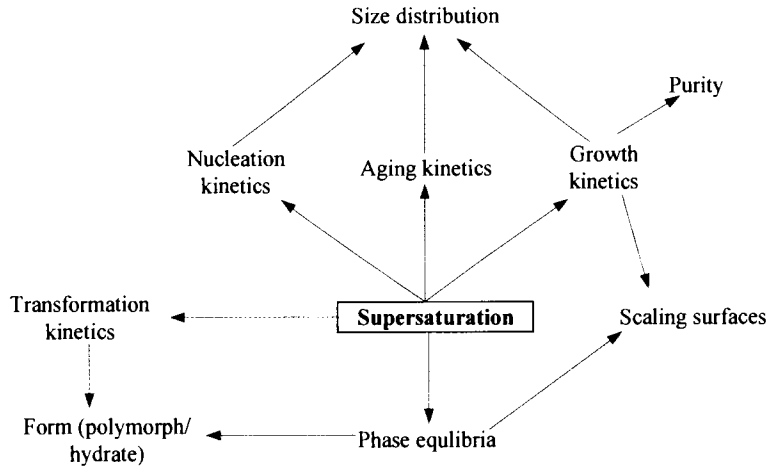


**Figure 3 - The role of supersaturation in precipitation processes (Sohnel and Garside, 1992)**

Supersaturation can be represented by equation 2 (Mohan and Myerson, 2002).

$$\frac{\Delta\mu}{RT} = \frac{\mu}{RT} - \frac{\mu_e}{RT} = \ln\left[\frac{a}{a^*}\right] \qquad [2]$$

Where $\mu$ is the solution chemical potential, $\mu_e$ is the solution chemical potential at equilibrium, $a$ is the activity coefficient, T is the temperature, $a^*$ is the equilibrium activity coefficient and R is the universal gas constant. The particle formation processes occurring in precipitation are nucleation, crystal growth, disruption, aggregation and other secondary changes. An illustration of the various precipitation mechanisms with respect to time is illustrated in Figure 4 below.

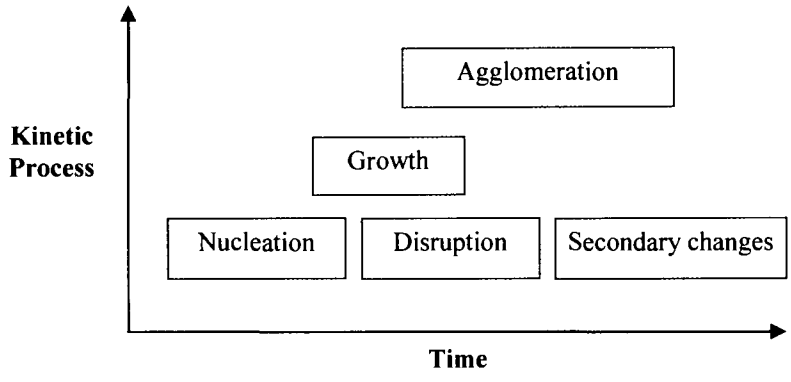


**Figure 4 – The range of time scale of precipitation mechanisms (Lewis and Kramer, 2008)**

### 2.1.1 Nucleation

When the concentration is increased under constant operating conditions, supersaturation increases as well. The increase of supersaturation is associated with an increasing tendency for solute ions to group. There is a point where the supersaturation becomes high enough for these groups of ions to grow into new stable solid particles. This process is called nucleation. Nucleation is thus the formation of the solid phase from nuclei which subsequently grows to produce tangible crystals (Jones, 2002; Mullin, 1972).

During precipitation, the chemical reaction results in the formation of single molecules of the precipitant, called monomers. As stated by Kashchiev (2003), nucleation occurs by the Szilard mechanism of successive attachments and detachments of single molecules (monomers) to and from the clusters of various size $n$ = 1, 2, 3 ....This formation of clusters can be represented schematically as follows:

$$[1] \Leftrightarrow [2] \Leftrightarrow [3] \Leftrightarrow \ldots \Leftrightarrow [n-1] \Leftrightarrow [n] \Leftrightarrow [n+1] \Leftrightarrow \ldots$$

Where, *[n]* denotes a cluster of $n$ molecules. Nucleation is therefore governed by the frequencies of monomer attachment and detachment from an n sized cluster (Kashchiev, 2003). Nucleation is successful when the cluster size exceeds a certain size ($n^*$) called the critical nuclei (which differs for different compounds). Clusters that are greater than n* are called super-nuclei and these are the particles seen in solution. The degree of supersaturation is the critical parameter controlling the rate of nucleation. The size of the

critical nucleus or cluster decreases with increasing supersaturation. Thus, the probability of the cluster surviving to form a stable crystal is higher.

Nucleation can be divided into two distinct groups, namely, primary nucleation and secondary nucleation with primary nucleation occurring through homogeneous or heterogeneous mechanism (Figure 5).

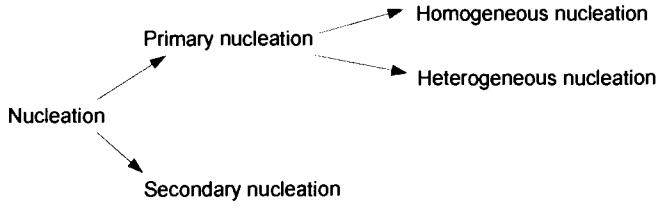


**Figure 5 - Mechanisms of nucleation (Sohnel and Garside, 1992)**

Figure 6 illustrates the relationship between supersaturation and the mentioned mechanisms of nucleation. The numbers denote the levels of supersaturation, with 1 being undersaturated region, 2 is low supersaturated region, 3 is high supersaturation region, 4 is very high saturation region and 5 is the ultra supersaturated region. Secondary nucleation is dominant in region 2 while primary nucleation is dominant in regions 3, 4 and 5.

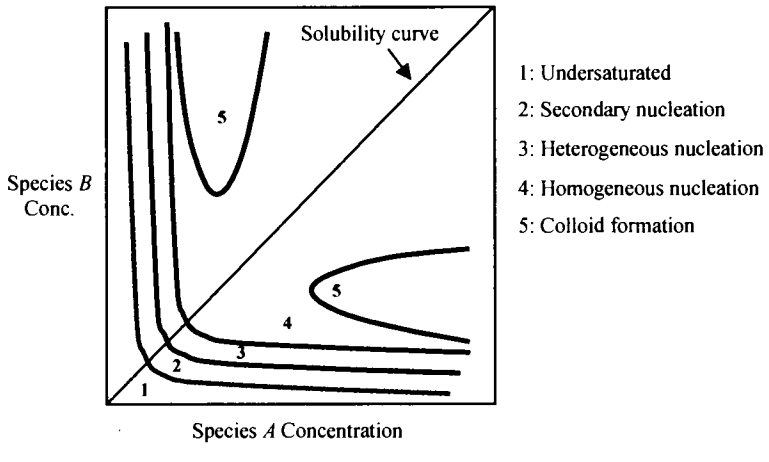


**Figure 6 – Effect of supersaturation on nucleation (Nielsen, 1979)**

Primary nucleation is reserved for all systems that do not contain product crystalline matter. It usually occurs at very high levels of supersaturation (regions 3, 4 and 5 in Figure 6). Primary nucleation can be further subdivided into homogeneous and heterogeneous nucleation. Homogeneous nucleation takes place under very high degrees

of supersaturation (region 4 in Figure 6). Very high supersaturation gives rise to ordered micro regions or clusters of molecules (Nielsen, 1979).

Heterogeneous nucleation takes place on foreign bodies. In industrial setup, it is rare to have conditions that favor purely homogeneous nucleation due to the presence of foreign surfaces like dust particles, solid impurities and crystallizer walls. Therefore, heterogeneous nucleation also plays a large part in primary nucleation in industrial practice. Heterogeneous nucleation takes place at lower supersaturation than homogenous nucleation (region 2 on Figure 6). The width of the metastable zone is smaller.

Secondary nucleation arises from the presence of crystals in the saturated solution. These crystals are called secondary nuclei. Secondary nuclei originate from the seed crystal (seeding) or from the boundary layer near the growing crystal. The presence of seeds in the solution catalyses the nucleation process by reducing the metastable zone hence nucleation takes place at a lower supersaturation (Myerson, 2002).

The seeds used can be either that of the mother crystals or foreign body crystals e.g. sand particles. Secondary nuclei can also originate from breakage or attrition of product crystals, hence at high stirring speeds this phenomenon is observed to be high. Another way to promote secondary nucleation is to recycle part of the mother liquor that contains crystals. These crystals will then act as secondary nucleation sites (Mersmann, 2001).

In order for nucleation to successfully take place, nucleation work needs to be overcome. Nucleation work is basically the energy barrier to the nucleation event. Liu (2001) defined nucleation as a process of the creation of critical size of nuclei, which results from surpassing the *nucleation barrier* (nucleation work), in terms of the fluctuation and growth of embryos. As stated earlier, nucleation is successful when the cluster size $n$ is greater than the size of the critical nuclei (denoted by $n^*$). If $n = n^*$, the system is in a metastable state. The assembling of these monomers into clusters involves a gain in work ($W_n$) (Kashchiev, 2000) given by:

$$W_n = -n\Delta\mu \qquad [3]$$

However, $W_n$ should contain a term accounting for the presence of an interface between the cluster and the ambient solution; hence equation 3 is modified to:

$$W_n = -n\Delta\mu + \Psi \qquad [4]$$

Where, ψ is equal to the cluster total surface energy. $W_n$ is maximum when the cluster is in its metastable state, that is, if $n = n^*$ (Kashchiev, 2000). At low supersaturations, the nucleation barrier is very high while at higher supersaturations, the exponential term associated with the nucleation barrier becomes less important (Liu, 2001).

The nucleation work is less for heterogeneous and secondary nucleation than for homogeneous nucleation (Liu, 2001; Kashchiev, 2000). This is because foreign bodies or seeds of the parent precipitant lower the interface energy (Richardson, 1994; Liu, 2001). Figure 7 shows the relationship between nucleation work and homogenous and heterogeneous nucleation.

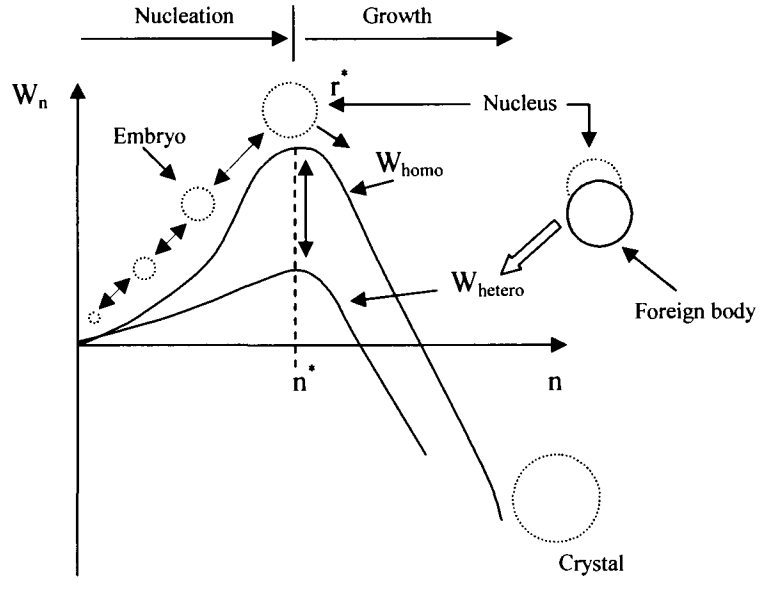


**Figure 7 – Illustration of the relationship between homogenous nucleation barrier ($W_{homo}$) and the effect of seeds or foreign bodies on this barrier (Liu, 2001).**

Liu (2001) stated that the kinetics of nucleation are not only determined by overcoming the nucleation barrier but also by the transport and kink integration at the surface of the embryo or growing cluster. Therefore, the addition of seeds will not only lower the nucleation barrier but also affect the transport of growth units to the surface of the growing clusters. However, this phenomenon is assumed to be negligible in the classical nucleation theories.

### 2.1.2 Classical nucleation theory

Kashchiev (2000) defined nucleation as the process of random generation of nanoscopically small formations of the new phase that have the ability for irreversible overgrowth to stable microscopic sizes. However, the clusters that are formed evolve and have a certain life span which depends on various aspects like the level of supersaturation and the size of the cluster itself (Kashchiev, 2000). The central problem in nucleation is the determination of the nucleation rate. The nucleation rate *J,* which has volume based units of $m^{-3}s^{-1}$, is the frequency of the appearance at time *t* (in seconds) of a stable cluster (super nuclei) per unit volume (Kashchiev, 2000).

$$J = \frac{dC_n(t)}{dt} \qquad [5]$$

Where, $C_n(t)$ is the concentration of nuclei in the system. The nucleation rate can be derived for three states, namely, the equilibrium, the stationary and the non stationary ones. For the equilibrium state, $J = 0$ while for the stationary state $J$ = *constant* and for the non-stationery state *J changes with time.* For the study of the nucleation kinetics of selenium precipitation, the stationary state is considered because the change in supersaturation is small over the residence time under consideration due to the small change in concentration of selenium (<2%) and the small solubility product ($10^{-57.7}$) of copper selenide).

Nucleation can take place through a homogeneous mechanism or a heterogeneous mechanism. It is important to be able to distinguish between these mechanisms for the purpose of understanding the precipitation process and this can be done by evaluation of the stationary nucleation rate. The stationary state requires a constant operating temperature and supersaturation. For supersaturation $S$ where ($S \geq 1$), the stationary nucleation rate $J$ is given by equation 6.

$$J = ASexp\left[\frac{-B}{\ln^2 S}\right] \qquad [6]$$

Where, $A$ is a kinetic quantity that determines whether the nucleation mechanism is homogenous or heterogeneous. In most cases A = $10^{13}$ to $10^{41}$ $m^{-3}s^{-1}$. A is practically

independent of the supersaturation (Kashchiev and van Rosmalen, 2003). The smaller values of this constant are indicative for the presence of foreign particles in the system (heterogeneous nucleation) while the higher values are indicative for homogenous nucleation. Determination of this kinetic factor in the selenium precipitation process is therefore important in order to determine ways to control and optimize the process. $B$ is a thermodynamic parameter that is related to the nucleation work ($W^*$) according to equation 7 and the nucleus size ($n^*$) according to the Gibbs-Thompson equation (equation 8).

$$\frac{W^*}{kT} = \frac{B}{ln^2 S} \qquad [7]$$

$$n^* = \frac{2B}{ln^3 S} \qquad [8]$$

Where $k$ is the Boltzmann constant and $T$ is the absolute temperature. The above relations are linked to supersaturation by the supersaturation ratio $S$. According to Sohnel and Garside (1992), the supersaturation ratio ($S$) of an electrolyte that dissociates in solution to give $v^+$ cations and $v^-$ anions is defined as:

$$S = \left[ \frac{m_+^{v+} m_-^{v-}}{m_{+.eq}^{v+} m_{-.eq}^{v-}} \right]^{1/v} \qquad [9]$$

Where $v = v^+ + v^-$, $m_+$ *and* $m_-$ are the concentrations of the cations and the anions respectively. The denominator to equation 9 is the solubility product of the solute ($K_{sp}$). Equation 9 is simplified to equation 10.

$$S = \left[ \frac{m_+^{v+} m_-^{v-}}{K_{sp}} \right]^{1/v} \qquad [10]$$

Because copper selenide dissociates according to equation 11 and its solubility product ($K_{sp}$) is $10^{-57.7}$ (OLI Stream Analyser Inc., 2004), the supersaturation ratio for the selenium precipitation process was therefore calculated according to equation 12.

$$Cu_2Se \leftrightarrow 2Cu^+_{(aq)} + Se^{2-}_{(aq)} \qquad [11]$$

$$S = \left[ \frac{[Cu^+]^2 [Se^{2-}]}{10^{-57.7}} \right]^{1/3} \quad [12]$$

Experimentally, the nucleation rate is not a directly measurable quantity. However it can be calculated by observing the change in concentration (equation 5) or change in number ($N_p$) of the super nuclei (observable particles) in the system. $N_p$ is a linearly increasing function of time ($t$) given by equation 13.

$$N_p = N_o + Jvt \quad [13]$$

Where $N_o$ is the super nuclei that are initially in the solution, $v$ is the volume of the system, $t$ is the residence time and $J$ is the nucleation rate. If the solution used is initially filtered to remove any particles, then $N_o$ is assumed to be negligible hence equation 13 becomes;

$$N_t = Jvt \quad [14]$$

Therefore a plot of $N_t/v$ versus time ($t$), for a specific value of supersaturation ($S$), should yield a straight line with slope equal to the nucleation rate ($J$). Apart from the degree of supersaturation, the rate at which new particles (super nuclei) are formed also depends on other aspects such as presence of foreign particles, line energy, strain energy, electric field, pressure of solution, concentration of pre-existing clusters and active centers. If foreign particles or clusters and active centers of the precipitate pre-exist, then the nucleation energy is reduced resulting in an increased particle formation rate (Kashchiev, 2000; Kashchiev and van Rosmalen, 2003). The effect of presence of foreign particles, and the concentration of pre-existing clusters and active centers is determined through the calculation of the nucleation kinetic constant (A). An increase in line energy and pressure results in the increase of the nucleation rate (Kashchiev, 2000). However, in this study, the line and strain energy and pressure are maintained constant as per process conditions. It is therefore important to fully understand the nucleation kinetics as they can be used to control the process. The knowledge of the nucleation rate helps to get a deeper understanding of the precipitation system which includes the induction time, the nucleus radius and the nucleus work.

### 2.1.3 Growth

The "birth of a new crystal" (nucleation) is followed by a process that further increases the size of the new crystal. This process is called crystal growth. Crystal growth is an important aspect in controlling the final particle size distribution obtained in a process. Size enlargement of the crystals is achieved by the deposition of growth units, preferably in layers.

Crystal growth is a diffusion and integration process, modified by the effect of the solid surfaces on which it occurs. Molecules or ions of the precipitant reach the growing faces of a crystal by diffusion through the liquid phase (Jones, 2002). Neither the diffusion step nor the interfacial step will proceed unless the solution is supersaturated. The rate of crystal growth can be expressed as the rate of displacement of a given crystal surface in the direction perpendicular to the surface. Mullin (1972) stated that different faces of a crystal grow at different rates under identical environmental conditions. In general, high index faces grow faster than the low ones. The overall crystal habit is determined by the slowest growing face (Mullin, 1972).

### 2.1.4 Aggregation and disruption

Aggregation is a process whereby very fine particles or crystals formed during precipitation are joined together by weak forces to form a larger particle. With time these particles will be firmly cemented by solid crystalline bridges. Most precipitation processes are agitated and this may lead to particle disruption thereby retarding aggregation and agglomeration. Aggregates are easily disrupted while agglomerates can only be disrupted and dispersed by crystal breakage attrition or erosion (Jones, 2002).

For agglomeration to take place the particles in the solution have to be transported and they have to collide. This can happen through Brownian motion, shear forces, difference in inertial forces and relative particle settling. Interparticle collision may then result in permanent attachment if the particles are small enough for the Van der Waals' forces to exceed the gravitational forces (Mullin, 1972).

### 2.1.5 Ostwald ripening

A precipitate produced by nucleation in a metastable supersaturated solution is far from thermodynamic equilibrium, i.e. a state of minimal free energy. A decrease of free energy is accomplished by a coarsening of the precipitate which essentially reduces the surface free energy with respect to the surrounding solution (Qin-bo et al., 2005). This process is called Ostwald ripening. The formation of many small particles (nucleation) is kinetically favored. However large crystals are thermodynamically favored. This is because small particles have a larger surface area to volume ratio than large crystals. Hence large particles, with their greater volume to surface area ratio, represent a lower energy state.

## 2.2 Reaction mechanisms

One of the many reasons for carrying out molecular modeling studies of a system is to establish the reaction transition states. Establishment of the transition states creates an understanding which paves the way for deriving ways to manipulate the reaction in order to improve the process. This may include addition of catalysts, changing the temperature or addition of other reagents. At the moment the selenium reduction process has neither known catalysts nor reagents that could increase the reaction time. Previous studies (Weir et al., 1982) were carried out at a higher temperature but the reduction time remained large. Therefore in order to identify the possible catalysts and better reduction reagents for the process, it is important to first get a fundamental knowledge of the behavior of these transition states.

Detailed analysis of how the chemical bonds break, intermolecular forces and how the ions interact to form transitional state compounds (complexes) is an aspect that must be considered during the study of reaction mechanisms. According to the transition state theory, many reactions proceed via a pre-equilibrium mechanism to produce transient intermediates known as "activated complexes". Polanyi et al. (1972) defined the transition state as the full family of configurations through which the reacting particles evolve en route from reactants to products.

Transition state complexes have similarities to both the reactants and the products (Asperger, 2003). Transient intermediates are very unstable and react quickly to form new products. Because of the short life of the activated complexes, determination of their

reaction rates is unrealistic. In most cases, the determination of the overall reaction constant is the logical way to gather any useful kinetic data. The mechanism of a reaction does not usually change with reaction conditions; it is a fundamental property of the reaction (Wojciechowski and Rice, 2003).

During chemical reactions, energy changes take place. The total energy of reactants is the sum of their kinetic and potential energies. Collisions between molecules results in transference of energy (breaking of bonds increase potential energy while bond formation lowers the potential energy). As a reaction proceeds, kinetic energy is converted into potential energy through bond stretching and molecular distortion. As a result, the transition state is the species of maximum potential energy (Asperger, 2003). The change in total Gibbs' free energy ($\Delta G$) at temperature $T$ is calculated from equation 15 as follows;

$$\Delta G\ (T) = E_o + ZPE + \partial H\ (T) - T^{*}\partial S\ (T) + E_{sol} \qquad [15]$$

Where $E_o$ is the total electronic energy (internal energy), ZPE is the quantum effect zero-point energy correction, $\partial H\ (T)$ and $\partial S\ (T)$ are the enthalpy and entropy changes of the system respectively. $E_{sol}$ is the solvation energy. The transition barrier or activation energy ($A_E$) can be calculated using equation 16.

$$A_E = \Delta G\ (TS) - \Delta G\ (R) \qquad [16]$$

Where $\Delta G\ (TS)$ and $\Delta G\ (R)$ are the total Gibbs free energies of transition state and reactant respectively.

There is no definite way for working out a mechanism but the proposed pathway should be consistent with general chemical principles (the reaction intermediate must be chemically possible) (Mortimer et al., 2002).

## 2.3 Selenium precipitation chemistry

The chemistry of selenium resembles that of sulphur due to their proximity within group 6 of the periodic table. Selenium is never found in its elemental state but it is rather associated with sulphide minerals (Tan, 2003). It has an atomic weight of 78.96 and an atomic number of 34. Due to its position in group 6 of the periodic table, selenium has characteristics of both metals and non-metals hence it has found many industrial applications as a semi-conductor.

Selenium, like sulphur, has four different inorganic oxidation states: (i) zero valence state (element selenium), which is highly insoluble in water, (ii) -2 valence state (selenide), which is the most reduced form of selenium, (iii) +4 oxidation state (selenite) and (iv) +6 oxidation state (selenate), which is the most oxidized form of selenium. The selenide ion is very unstable and is readily oxidized to element selenium in water (Maiers et al., 1988). Selenites and selenates are the major contaminants of the copper leach solution due to their high level of solubility in water (Séby et al., 2001). Selenates are predominant at high redox potentials and not easily reduced because of their low adsorption and/or precipitation capacities (Elrashidi et al., 1987).

Selenites on the other hand are easily reduced (Elrashidi et al., 1987). In the moderate redox range, selenite is the predominant species while selenide ($Se^{2-}$) is thermodynamically stable under strongly reducing environments and exists as metal selenides (Séby et al., 2001).

### 2.3.1 Selenium precipitation processes

There are many methods used to remove selenium from solutions depending on the industry in which this element is an impurity. The technologies for the removal of selenium can be classified into physical treatment, chemical treatment and biological reduction. The processes that fall under physical treatment are; coagulation, adsorption, ion exchange and membrane separation. Sorg and Logsdon (1978) deduced that selenium (+4) can be effectively reduced when ferric sulphate is used as the coagulant in pH range 6-7. Adsorption of selenium (+4) by ferrihydrite and alumina can also reduce the selenium concentration to accepted levels (Merril et al, 1987; Trussel et al., 1980). Efforts to investigate the removal using ion exchange were carried out by Maneval et al.,

(1985) and they deduced that Se (+4) can be removed more effectively than Se (+6) using a strong base anion exchange resin. However this process is hampered by ions such as sulphates which may load preferentially. Membrane separation can be viable but is only suited to treat drinking water instead of acidic mine solution (Twidwel et al., 1999).

The removal of selenium through chemical treatment is common and has been studied extensively in waste water treatment. Murphy (1988) patented a process that could reduce Se (+4) and Se (+6) ions to element selenium by using ferrous hydroxide as the reducing agent at pH 9 (Zingaro et al., 1997). Se (+6) can also be successfully removed if iron is used as a reductant, catalysed in the presence of copper to produce elemental selenium, iron selenide or hydrogen selenide (McGrew et al., 1996). Reduction using metallic copper, nickel or iron at high pressure is another suggested route for selenium removal (Sharmasarkar et al., 1996; Zingaro and Cooper, 1974). The use of a fluidised bed of elemental copper to precipitate selenium was proposed by Zingaro and Cooper (1974). The copper electrolyte is passed through a column in the upward direction through a bed of copper granules. Selenium is then precipitated out as copper selenide and can be removed by filtration.

The use of bacteria has been extensively studied and shows great potential (Lupton and Sheridan, 2008). However, this process is extremely slow with residence times ranging from days to months.

The disadvantage of most of the above mentioned methods is that they cannot reduce the selenium to the required levels of less than 1ppm in the final copper cathode. Most of these methods may require that all the aqueous selenium be present in the Se (+4) oxidation state rather than Se (+6) (Nikolic and Laferty, 1981). Reduction of selenium using sulphur bearing reductants (e.g. sodium sulphite and sulphur dioxide) is the most effective route. The reduction using sodium sulphite is preferred over sulphur dioxide because sodium sulphite is safer to handle in an industrial process. The reported extent of reduction is lower for selenate than for selenite (Maiers et al., 1988). Zingaro and Cooper (1974) also reported that selenate cannot be reduced by treatment with sulphur dioxide at atmospheric pressure except in the presence of a catalyst such as halide or thiourea. However, the use of such catalysts is not desirable in the electrowinning solution as it

results in an increase of chloride ions in the electrolyte. High chloride ion concentration is not desirable as it results in poor physical quality of the cathodes, low current efficiencies and high corrosion rate of plant equipment.

### 2.3.2 Reduction using sodium sulphite

Removal of selenium from copper sulphate solution using sulphur based reductants was studied by Clark and Rickard (1975), Hofirek (1981), Nikolic and Laferty (1981) and Weir et al. (1982). The process being investigated in this study was suggested by Weir et al. (1982). In this process the acidic copper sulphate is heated to a temperature of 95°C and reacted with sodium sulphite in a tubular reactor at atmospheric pressure. Copper selenide is precipitated from the solution. However, the solution also contains dissolved cuprous ions which can cement out on cooling. To avoid this taking place, the temperature of the treated mixture is maintained at 95°C and air is passed into the solution to oxidize the dissolved cuprous ions to cupric ions ($Cu^{2+}$). The solution is cooled and copper selenide is filtered out (Hofirek, 1981).

*2.3.2.1 Chemical reactions and reaction mechanism*

Elrashidi et al. (1987) reported that ($HSeO_3^-$) and ($HSeO_4^-$) were the most stable selenium species under acidic environments. Both these selenium species are soluble in copper sulphate solution as depicted by their low $pK_a$ values in equations 17 and 18 respectively (Séby et al., 2001).

$$H_2SeO_3 + H_2O = HSeO_3^- + H_3O^+ \quad pKa = 2.57 \qquad [17]$$

$$H_2SeO_4 + H_2O = HSeO_4^- + H_3O^+ \quad pKa = -1.97 \qquad [18]$$

The proposed reaction mechanism for selenium precipitation in the copper sulphate solution is depicted in Figure 8. The following reactions take place during selenium precipitation: (i) reduction of $Cu^{2+}$ to $Cu^+$ (ii) reduction of selenite and selenate to selenide (for selenate, the path follows the dotted line) and (iii) reaction of the cuprous ion with the selenide ion to form the precipitate ($Cu_2Se$).

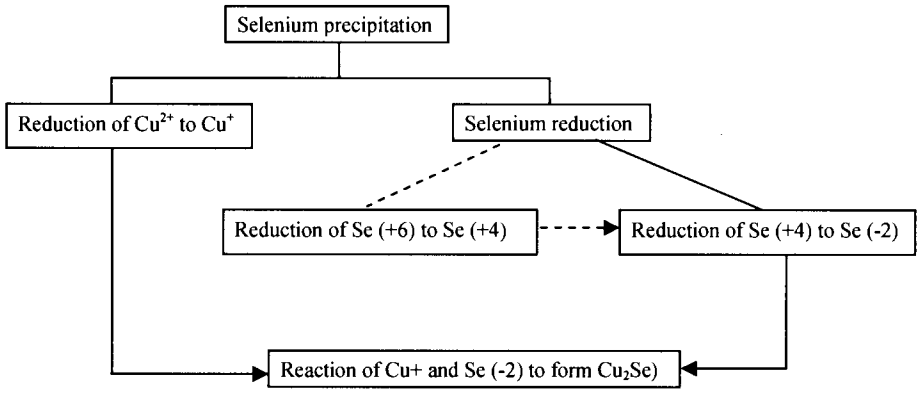


**Figure 8 – Reaction mechanism for selenium precipitation**

*2.3.2.2 Reduction of cupric ion*

Addition of the highly reducing sodium sulphite results in reduction of the cupric ion ($Cu^{2+}$) to the cuprous ion ($Cu^{+}$) (equation 19). This reaction can take place at temperatures as low as ambient temperature (Hofirek, 1981).

$$Cu^{2+}_{(aq)} + HSO_3^-{}_{(aq)} + H_2O = Cu^{+}_{(aq)} + HSO_4^-{}_{(aq)} + 2H^{+}_{(aq)} \quad [19]$$

However in aqueous solutions, the cuprous ion is unstable and has a tendency to disproportionate to form cupric ion and metallic copper according to reaction 20 (Habashi, 1993).

$$Cu^{+}_{(aq)} \leftrightarrow Cu^{2+}_{(aq)} + Cu\downarrow \quad [20]$$

This reaction is undesirable and will need to be controlled. Hofirek (1981) proposed that the cuprous ion can be stabilised by operating at a temperature between 140°C and 150°C.

*2.3.2.3 Reduction of selenate and selenite*

The other reaction in selenium precipitation process involves the reduction of selenite and selenate to selenide ions. This involves two steps for selenate. The sequence of reduction from Se (+6) to the selenide ion is depicted in Figure 9.

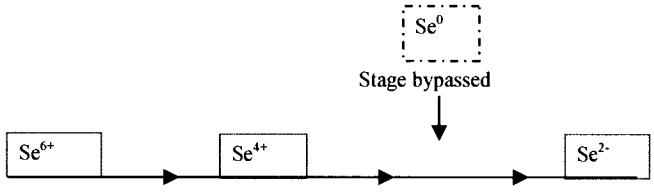


**Figure 9 – Sequence of selenate reduction**

The reduction sequence skips the intermediate solid selenium element because selenium is not formed in the presence of cupric ions (Hofirek, 1981). The reduction of selenate takes place as shown by equation 21.

$$HSeO_4^-{}_{(aq)} + 2H^+{}_{(aq)} + 2e^- = HSeO_3^-{}_{(aq)} + H_20 \quad [21]$$

Reaction 23 has a standard potential of 1.008 V (Séby et al., 2001). Thermodynamic data suggests that this reaction is spontaneous and is especially so at low temperatures. However, this reaction is the slowest and therefore is the rate limiting step (Brimmer et al., 1987; Elrashidi et al., 1987; Hofirek, 1981). In contrast, the reduction of selenite to selenide is fast (Elrashidi et al., 1987; Fujita et al., 2005; Hofirek, 1981). Selenite reduction takes place according to equation 22.

$$HSeO_3^-{}_{(aq)} + 6H^+{}_{(aq)} + 6e^- = HSe^-{}_{(aq)} + 3H_2O \quad [22]$$

Equations 21 and 22 show why there is need to keep an acidic environment in the reactor (a high proton concentration will shift the equilibrium to the right).

*2.3.2.4 Copper selenide formation*

Hydrogen selenide ($HSe^-$) produced in equation 22 is very stable under reducing conditions at a pH below 3.8 (Linkson, 1992). However, in the presence of $Cu^+$ ions, the selenide ion becomes very unstable and reacts to form a highly insoluble precipitate (copper selenide) according to reaction 23.

$$2Cu^+{}_{(aq)} + HSe^-{}_{(aq)} = Cu_2Se\downarrow + H^+ \quad [23]$$

$$H_2SeO_4 + 5Na_2SO_3 + 2CuSO_4 + H_2O = Cu_2Se + 5Na_2SO_4 + 2H_2SO_4 \quad [24]$$

The overall stoichiometric equation for selenium precipitation using sodium sulphate as the reductant is given by equation 24.

### 2.3.3 Copper reactions in the reduction process

Copper reactions with both sulphite and selenide ions play a significant role in the precipitation of selenium. It is therefore important to understand the subsequent reactions that copper undergoes throughout the reduction process. According to Conklin and Hoffman (1988), copper forms complexes in the reaction mixture and these complexes undergo a series of redox reactions that result in an aqueous mixture of $Cu^{+}$, $Cu^{2+}$, $SO_4^{2-}$ and $SO_3^{2-}$. The sulphite ions reduce $Cu^{2+}$ according to the following reaction in non acidic solutions (Conklin and Hoffmann, 1988).

$$2Cu^{2+} + SO_3^{2-} + H_2O \rightarrow 2Cu^{+} + SO_4^{2-} + 2H^{+} \quad [25]$$

It is important to note that the sulphite ions are responsible for the reduction of both selenate and selenite including $Cu^{2+}$. The reduced copper species ($Cu^{+}$) will then react with the reduced selenium species ($Se^{2-}$) according to reaction 25. Since the copper sulphate solution is acidic, sodium sulphite dissociates to hydrogen sulphite ions ($HSO_3^{-}$) and equation 26 describes the equilibrium relationship in solution (Conklin and Hoffmann, 1988).

$$HSO_3^{-} \leftrightarrow H^{+} + SO_3^{2-} \quad [26]$$

A yellowish brownish cupric ion - sulphite complex is formed instantly on mixing according to equation 27 (Conklin and Hoffmann, 1988).

$$Cu^{2+} + SO_3^{2-} \leftrightarrow CuSO_3 \quad [27]$$

The cupric sulphite complex intermediate formed is very unstable and a rapid reduction of the cupric ion to cuprous ion ($Cu^{+}$) takes place with the sulphite being oxidized to the sulphate ion according to equation 28 (Conklin and Hoffmann, 1988).

$$Cu^{2+}(C^{*}) + SO_3^{2-} \leftrightarrow Cu^{+} + SO_4^{2-} \quad [28]$$

Where *(C*)* is a sulphite entity of the intermediate complex. In the presence of selenide ions in solution, the synthesis of copper selenide is then initiated.

# 3.0 EXPERIMENTAL

## 3.1 Thermodynamic simulation

Before bench-scale experiments could be carried out it was important to predict the behaviour of the process under real world conditions. This includes predicting all chemical species involved in the reactions and the products of the reactions. This was carried out using predictive aqueous modelling tools, OLI Stream Analyser (OLI system Inc., 2004) and HSC Chemistry 5.11 (Outokumpu Research., 2002). The OLI thermodynamic framework is based on the combined work of Bromley, Zemaitis, Meissner, Pitzer, and OLI technologists (Rafal et al. 2001). The Eh-pH-module in HSC Chemistry 5.11 is based on Stability Calculations for Aqueous Systems (STABCAL), developed by H.H. Haung, 1989 (Outokumpu Research., 2002).

The objective of carrying out a thermodynamic analysis of the process is to establish speciation in the copper sulphate solution at the operating conditions of 95°C and 1 atmosphere. Thermodynamic data may be used (i) to predict the type of chemical species that are stable at the process operating conditions, (ii) to predict the compounds that will precipitate out when the reductant (sodium sulphite) is added into the acidic copper sulphate solution and (iii) to determine conditions likely to be favourable to the precipitation of selenium.

## 3.2 Reaction time

The objective of these experiments was to determine the reaction time for both selenite and selenate reduction. This information is important in confirming the rate determining step in the selenium reduction process. The experiments also investigated whether $Se^{4+}$ has any catalytic effect on $Se^{6+}$ precipitation.

### 3.2.1 Materials and chemicals

Analytical grade chemicals were used for all the experiments. The chemicals included; sodium selenite ($Na_2SeO_3$), sodium selenate ($Na_2SeO_4$), sodium sulphite ($Na_2SO_3$), copper sulphate pentahydrate ($CuSO_4.5H_2O$) and concentrated sulphuric acid (98% $H_2SO_4$).

### 3.2.2 Experimental set-up

The bench-scale experiments to investigate the reactivity of Se(+4) and Se(+6) were conducted in a temperature-controlled glass reactor (Figure 10). The glass reactor had baffles and had an overhead stirrer for agitation. The reaction temperature was monitored and controlled via a thermocouple connected to a Gefran temperature controller that controlled the heating jacket. The experiments were carried out at 95°C and at atmospheric pressure. A reflux condenser was installed on the reactor to prevent water loss through evaporation. In order to avoid the change in volume due to sampling having an effect on the experimental results, the total sample volume was kept below the allowable limit i.e. a quarter of the reactor contents (in the experiment it was kept below 15% of the reactor volume).

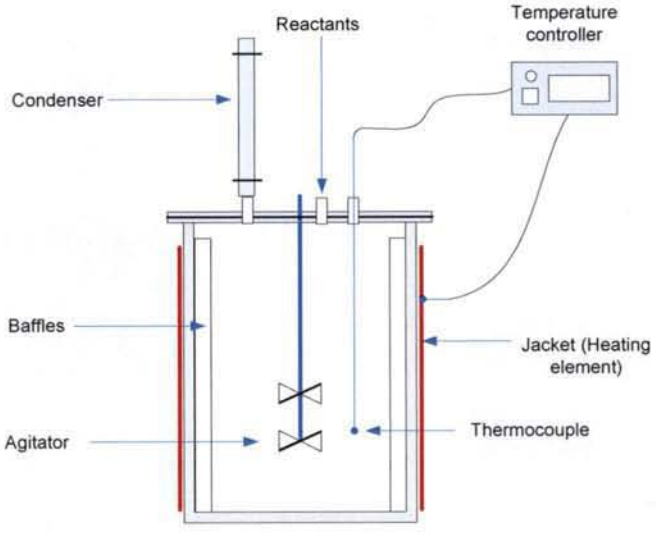


**Figure 10– Schematic view of the batch reactor used during the experiments**

### 3.2.3 Experimental procedure

Three outcomes were desired from the experiments (i) determination of the rate of selenium (+4) precipitation, (ii) determination of the rate of selenium (+6) precipitation and (iii) determination of the rate of selenium precipitation with a mixed valence solution (with $Se^{+4}$ and $Se^{+6}$ in solution).

A synthetic copper sulphate solution was prepared to simulate the process stream and it had the following specifications: 0.315M copper sulphate pentahydrate, 0.41M sulphuric

acid and 100mg/l selenium (+4) for the first experiment, 100mg/l selenium (+6) for the second experiments and 50mg/l of each for the third experiment. A synthetic solution of 0.762mol/l sodium sulphite was also prepared for use as a reductant on all the experiments.

In each experiment, 400ml of the synthetic copper sulphate solution was filled in the glass reactor and heated to a temperature of 95°C. Twenty millilitres (20 ml) of sodium sulphite (preheated to 95°C) was added in the reactor to precipitate selenium. Samples (5 ml) were drawn from the reactor at one minute intervals for the first experiment, 6 hour intervals for the second experiment and ten minute intervals for the third experiment. Each sample was diluted in 200 ml distilled water (temperature less than 5°C), to quench the reaction. The quenched sample was then filtered and the filtrate was analysed for selenium. The residues were also collected for analysis.

### 3.2.4 Analysis

Analysis of selenium was carried out using inductively coupled plasma mass spectroscopy (ICP-MS). The residues were also collected for X-ray diffraction (XRD) and scanning electron microscope (SEM) analysis.

## 3.3 Significance of copper interactions with sulphite ions

In previous experiments to determine the reaction time of the selenate and selenite ions, there were sudden colour changes immediately after addition of sodium sulphite into the reactor. It was therefore important to understand the copper redox reactions taking place including the transitional compounds formed. This information will not only help understand the process better but will also help significantly in further studies to come up with ways to speed up the reduction reaction. The objective of these experiments was therefore to investigate the complex redox reactions resulting from the interaction of copper ions and sulphite ions and to get an understanding on their effect on the overall process.

### 3.3.1 Procedure

Analytical grade reagents from Merck South Africa were used in the experiment. These are sodium sulphite, copper sulphate (pentahydrate), concentrated sulphuric acid. Triple

distilled water was used for the preparation of all the solutions. A temperature controlled water bath was used to maintain the temperature at 95°C.

The following synthetic solutions were prepared: copper sulphate solution with the following specifications; 0.5M copper sulphate, 0.4M sulphuric acid and 0.5M sodium sulphite.

Ten milliliters (10 ml) of both the copper sulphate solution and sodium sulphite were placed in different test tubes. The test tubes were placed in the water bath and left until the solution temperatures were steady at 95°C. The sodium sulphite in one test tube was then reacted with the copper sulphate in another test tube. Colour transformations were observed. The second experiment involved using excess sodium sulphite (15ml instead of 10ml). Again colour transformations were observed.

### 3.3.2 Analysis

Samples of the mixtures were also taken for SEM and XRD analysis.

## 3.4 Molecular modeling

A molecular modeling approach was used to provide a fundamental understanding of the differences in the reactivity of the selenium species $SeO_3^{2-}$, $SeO_4^{2-}$ and the protonated ions $HSeO_4^-$ and $HSeO_3^-$. Such a method has been used with success to investigate reactivity and chemical reaction mechanisms of different species at a molecular level (Ma et al., 2008). The redox reactions to be investigated are the $SeO_4^{2-} \rightarrow SeO_3^{2-}$ and $HSeO_4^- \rightarrow HSeO_3^-$ reduction steps.

Geometry optimization of the reactants, intermediates and products was performed using B3LYP flavor of the density functional theory (DFT) in the commercial program Jaguar 7.5 (Schrodinger, Inc., Portland, OR). The LACVP** basis set was used for all computations. All optimized geometries of the reactants and products were positively identified for local minima (the frequencies were verified to be real i.e. zero imaginary frequencies). The transition state geometries were characterized by the existence of a single imaginary frequency.

Computation of vibrational frequencies was performed at all optimized geometries (reactants, transition states and products) to obtain zero point energies (ZPE) and the

relevant thermodynamic parameters (enthalpy, entropy and free energy). Solvation energy ($E_{sol}$) was calculated by including solvation effects using the continuum-solvation technique with the Poisson–Boltzmann (PB) approach. The dielectric constant $e$ = 80.37 and a probe radius $r$ = 1.40Å were used for the water as solvent. All calculations were performed assuming a temperature of 95°C and one atmosphere pressure.

### 3.5 Nucleation kinetics

The objective of these experiments were to determine nucleation kinetics of selenium (+4) precipitation from acidic copper sulphate using sodium sulphite as the reductant.

#### 3.5.1 Reagents

All the chemicals used were analytical grade Merck Chemicals. These included sodium selenite ($Na_2SO_3$) in powder form, copper sulphate pentahydrate ($CuSO_4.5H_2O$) in solid form and concentrated sulphuric acid (98% $H_2SO_4$).

#### 3.5.2 Experimental set-up and procedure

A synthetic solution of copper sulphate with the following specifications was prepared: 0.315M $CuSO_4$ and 0.41M $H_2SO_4$. The concentration of selenium in the copper sulphate solution was varied by dissolving sodium selenite to make up the required concentration (20ppm for the first experiment, 50ppm for the second, 100ppm for the third and 1000ppm for the last experiment). A 0.095M solution of sodium sulphite was also prepared.

Figure 11 shows the schematic diagram of the experimental set-up. The experiments were carried out in a Y-mixer and tubular reactor configuration. The geometry of a Y-mixer promotes rapid mixing down to molecular scale, which is a requirement before nucleation starts (Roelands et al. 2005). The Y-mixer has been used successfully in previous studies (Mahajan and Kirwan, 1993; Roelands et al. 2005; Blandin et al. 2001) and is suitable for such studies.

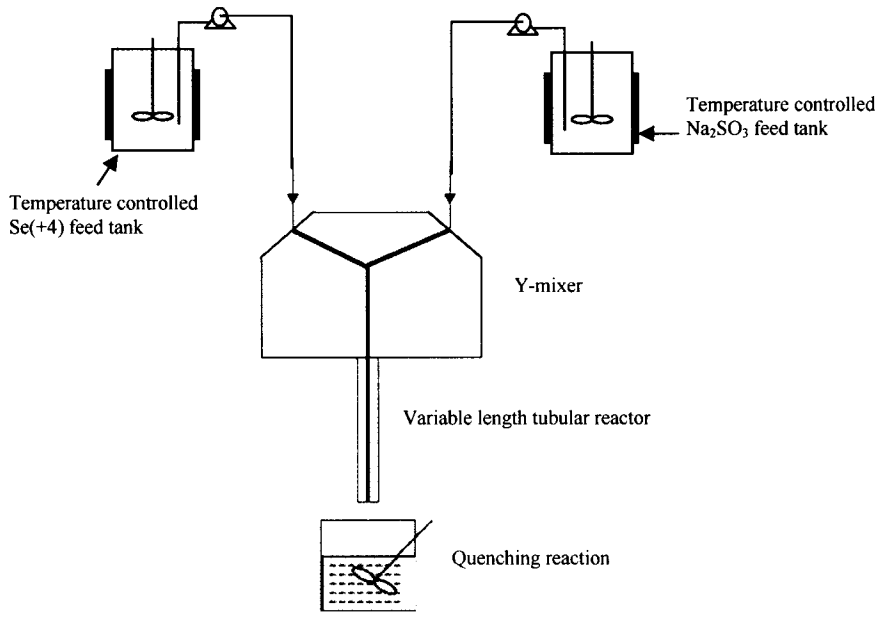


**Figure 11 – Layout principle of set-up for nucleation rate determination**

A Y-mixer with an angle of 160° between the reagents inlets was used. The internal diameter of the two inlets and the outlet to the Y-mixer were 3mm. A peristaltic pump was used to inject the two feed streams into the Y-mixer inlets. Equal flow rates (650 $cm^3$/min) for both sodium sulphite and copper sulphate solution containing selenium was used. De-ionised water was used in all the experiments to reduce contamination of the solution by foreign particles. The feed solutions were heated to a temperature of 95°C under atmospheric pressure.

The nucleation rate was determined for four different supersaturation ratios: $8.66x10^{15}$, $2.17x10^{16}$, $4.32x10^{16}$ and $4.33x10^{17}$. These supersaturation levels corresponded to selenium concentrations of 20ppm, 50ppm, 100ppm and 1000ppm respectively. For each value of supersaturation, the number of particles was measured for tube lengths of 0.5m, 1.0m, 1.5m and 2.0m. These tube lengths corresponded to residence times of 0.81s, 1.58s, 2.34s and 3.11s respectively. The diameter (D) of the tubes used was 6.5mm. Under these experimental conditions, the Reynolds number in D=6.5mm is 4500; hence it can be assumed that fully developed turbulent plug flow exists in the tubular reactor lengths used in the study.

In order to justify the use of the stationery rate, the supersaturation ratio was calculated before the reaction commenced and after a residence time of 3.11s. The results (Table 1) showed that the maximum change in the supersaturation took place when the initial supersaturation ratio was $8.66x10^{15}$ (1.1% decrease).

**Table 1 – Change in supersaturation over the experimental residence time of 3.11s**

| Initial supersaturation | % Decrease in supersaturation |
|---|---|
| $8.66x10^{15}$ | 1.10 |
| $2.18x10^{16}$ | 1.00 |
| $4.32x10^{16}$ | 0.90 |
| $4.33x10^{17}$ | 0.92 |

Supersaturation changes of the same order have been used in previous studies (Roelands et al. 2005; Mahajan and Kirwan, 1993). It was therefore assumed that the supersaturation over the experimental duration was constant. The main reason for the insignificant change is the small change in the selenium concentration over the experimental residence time and the high pKa of copper selenide ($10^{-57.7}$).

### 3.5.3 Sampling and measurements

A 108ml sample was collected from the outlet tube into a container filled with de-ionised water. Dilution of the sample with two litres of de-ionised water at room temperature was carried out in order to quench the reaction and hence prevent additional nucleation. The effectiveness of the dilution was checked by carrying out a PSD analysis immediately after collection of the sample and then 7 minutes after collection of the sample. The PSD was invariant for the dilution using two litres of de-ionised water; hence it was determined that this dilution ratio was effective in quenching the reaction for the period required to take a measurement (7 minutes in this case). A 2ml sample was taken and analysed for the number of particles ($N_p$). This procedure was repeated for four different lengths of the outlet tubes and for four different supersaturations. The number of particles was analysed using the dynamic light scattering (DLS) technique (Nano ZS, Red badge, Model: ZEN 3600).

# 4.0 RESULTS AND DISCUSSION

## 4.1 Thermodynamic simulation

### 4.1.1 Aqueous phase properties

Table 2 shows the aqueous phase properties of the initial copper sulphate solution at 95°C and 1 atmosphere. The species in the initial copper sulphate solution are shown in Appendix A. The values were created using OLI Stream Analyser (OLI system Inc., 2004).

**Table 2 – Aqueous phase properties of the process feed at 95°C and 1 atmosphere**

| | |
|---|---|
| pH | 1.93 |
| Ionic strength | 0.10 mol/mol |
| Solution density | 1.19 g/ml |
| ORP | 0.94 V (SHE) |

The solution is highly oxidised (ORP 0.94V). This is expected because during the leaching process, oxygen is injected into the system in order to oxidise copper to copper oxide. During this process, selenium is also oxidised to selenites and selenates. The initial solution contains the aqueous phase only, with the dominant aqueous species being $H^+$, $SO_4^{2-}$, $HSO_4^-$, $HSO_3^-$ and $Cu^{2+}$. These results are in agreement with previous studies (Elrashidi et al., 1993) showing that under acidic and oxidising conditions, selenium exists as hydrogen selenate and hydrogen selenite ($HSeO_4^-$ and $HSeO_3^-$ respectively).

Figure 12 shows the behaviour of the initial copper sulphate solution with changes in pH. This was modelled using OLI Stream Analyser (OLI system Inc., 2004).

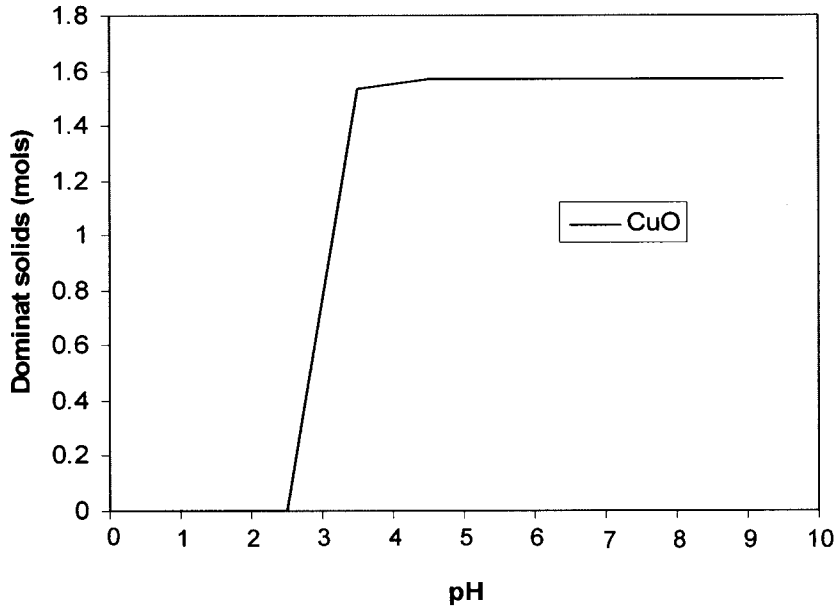


**Figure 12 - Solids formed in initial copper sulphate solution with changes in pH at 95°C, 1 atm**

The graph shows that the initial copper sulphate solution, at pH 1.93, does not contain any solid phases. However, increasing the pH favours the precipitation of copper oxide, which starts to precipitate at pH 2.5.

### 4.1.2 Potential/pH (Eh/pH) diagrams

It is essential to identify the predominant aqueous species in the copper sulphate solution before the reduction reaction. Establishment of the boundaries of the selenium precipitation system in a potential/pH diagram results in the formation of domains in which a particular species is thermodynamically stable. The process of establishing the Eh/pH diagram for the overall system was carried out by construction of the species – water system for all species in the copper sulphate solution and then superimposing them on each other (modelled using OLI Stream Analyser, 2004). Figure 13 illustrates the Se–$H_2O$ system at 95°C and atmospheric pressure (modelled using HSC Chemistry 5.1).

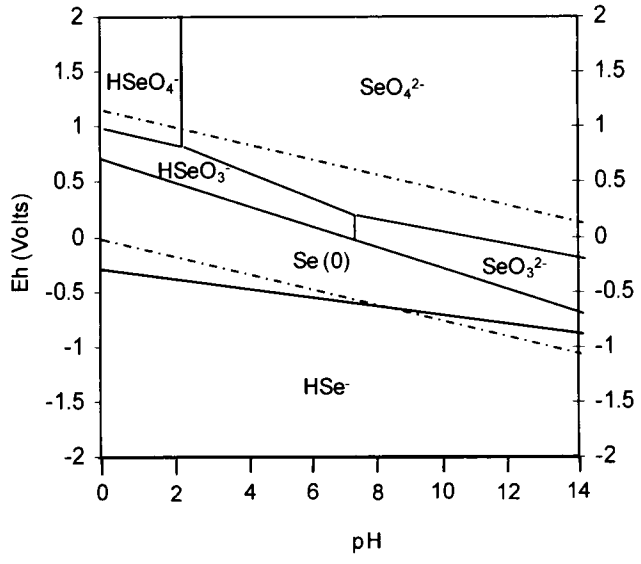


**Figure 13 – Potential/pH diagram for Se – $H_2O$ systems at 95°C and 1 atmosphere**

Since the initial process solution has a pH of 1.93 and a potential of 0.94V, it lies in the region marked $HSeO_4^-$ on the Eh/pH diagram. This shows that the dominant selenium species in the copper sulphate solution under the operating conditions is $HSeO_3^-$. This is in agreement with results from the OLI thermodynamic model. Figure 14 shows the speciation diagram for copper (modelled using HSC Chemistry 5.1).

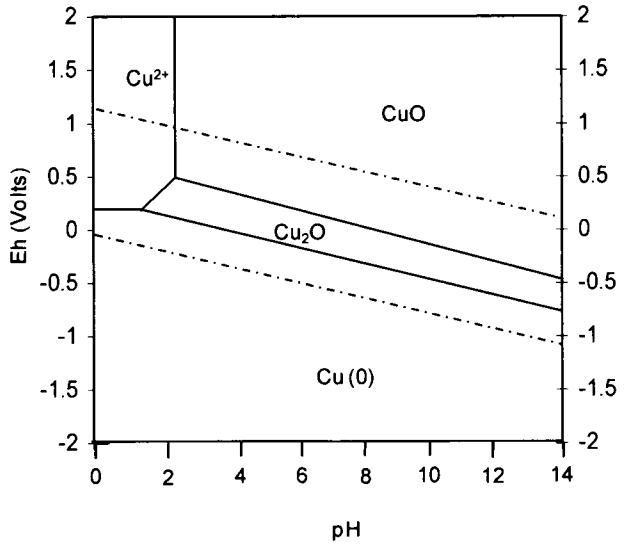


**Figure 14 – Potential/ph diagram for Cu – $H_2O$ systems at 95°C and 1 atmosphere**

The cupric ions are stable over a small pH range (between zero and three) and at high potential (between 0.35V and 2V). Increasing the pH above 3 under highly oxidising conditions favours precipitation of CuO. Copper (I) oxide ($Cu_2O$) is formed under mild reducing conditions while under highly reducing conditions solid elemental copper is thermodynamically stable. However, in the copper sulphate solution, selenium and copper ions co-exist. Therefore, a combined Eh/pH diagram will give the overall speciation of the system. The overall Eh/pH diagram is shown in Figure 15.

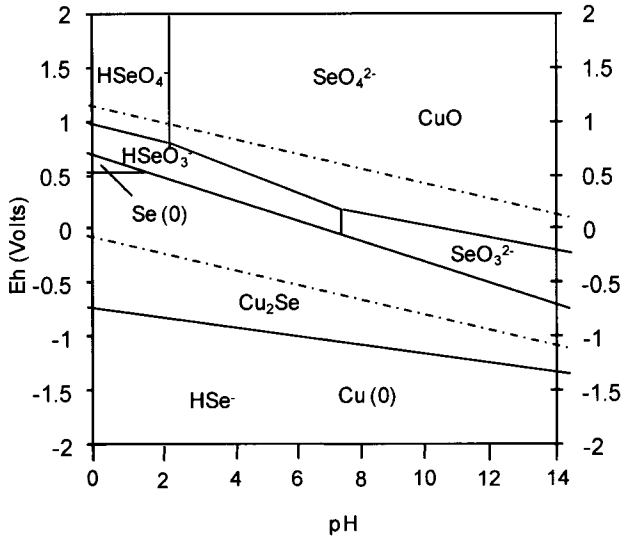


**Figure 15 – Potential/ph diagram for Se –Cu – $H_2O$ systems at 95°C**

The speciation diagram reveals that copper selenide ($Cu_2Se$) is formed over the whole range of pH under reducing conditions only. The reducing condition in the precipitation reaction is induced by addition of sodium sulphite. A thermodynamic survey by pH was carried out using OLI Aqueous Stream Analyser (OLI system Inc., 2004) to predict the dominant solids formed when sodium sulphite is added to the copper sulphate solution. The results are shown in Figure 16. The aqueous species output of the system after sodium sulphite addition is shown in Appendix 2 (OLI system Inc., 2004).

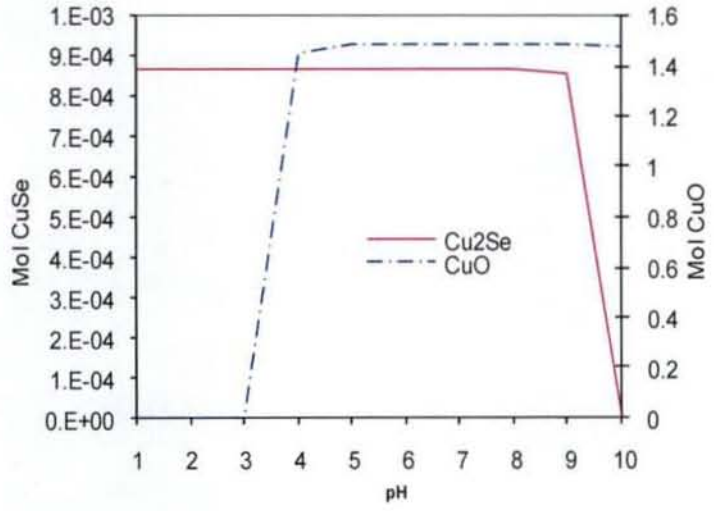


**Figure 16 - Thermodynamic simulation for selenium precipitation at 95°C.**

The graph shows that when sodium sulphite is added to the initial copper sulphate solution (containing selenium as an impurity), copper selenide ($Cu_2Se$) precipitates out between pH 1 and pH 9. From pH 9 upwards, selenium re-dissolves into solution. Copper oxide (CuO) starts to precipitate at pH 3. It is therefore important to keep the pH below 3 to ensure the precipitation of copper selenide only. Since the initial copper sulphate solution has a pH of 1.93, only copper selenide is guaranteed to precipitate on reduction.

### 4.1.3 Thermo-chemical calculations

Figure 17 and 18 shows the enthalpy changes and the change of equilibrium constants with temperature for the reactions taking place during selenium precipitation respectively (modeled using HSC Chemistry 5.1).

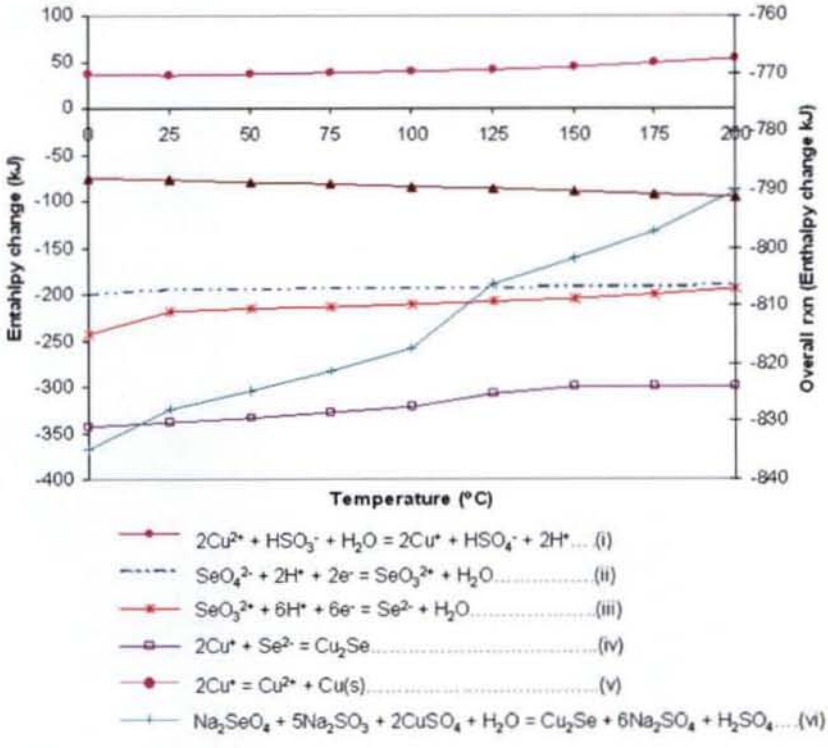


**Figure 17 - Enthalpy change for reactions taking place during Se precipitation**

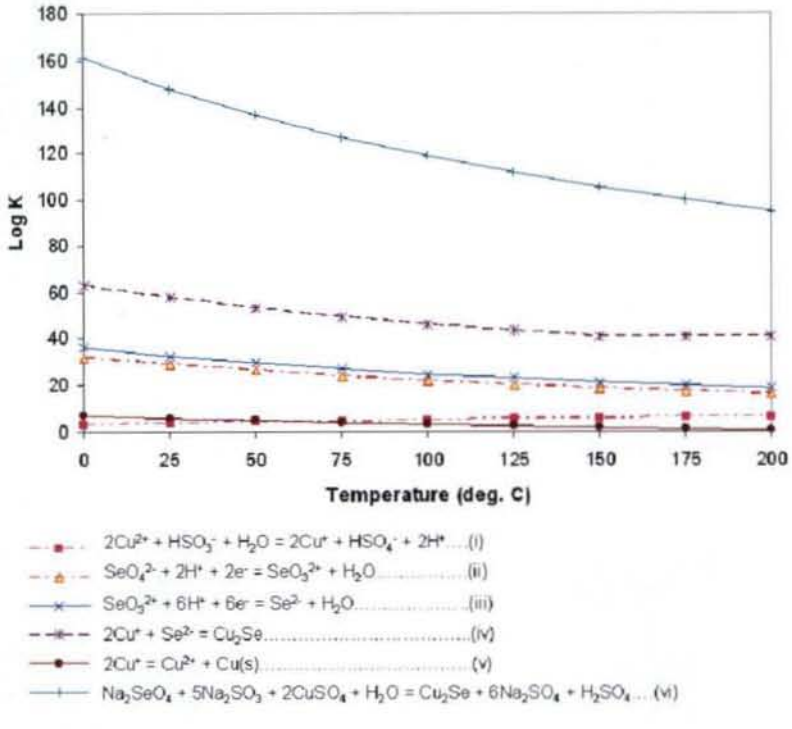


**Figure 18– Equilibrium constant for reactions taking place during Se precipitation**

Figure 17 shows that the reduction step (reaction i) is thermodynamically feasible and has a negative Gibbs free energy. The negative Gibbs free energy predicts that the reaction is spontaneous while the positive logK shows that the reaction goes forward to completion. This reaction is more favourable at high temperatures. Reaction iv (disproportionation reaction) is undesirable and an increase in temperature results in the disproportionation reaction being discouraged. Therefore, the cuprous ion can be stabilised by operating at high temperatures.

Figure 18 also shows that for reactions ii, iii and v, the forward reaction is highly favored at low temperatures (logK decreases with an increase in temperature). Hence, as stated before, operating at a temperature between 85°C and 100°C is reasonable in order to optimize the process. HSC Chemistry gives an equilibrium constant value of approximately $10^{-57.7}$ for reaction 4. This result is in agreement with that reported by Elrashidi et al., (1987) who gave a value of $10^{-60.8}$ under similar conditions.

### 4.2 Reaction time

Figure 19 shows the results of the batch experiments carried out to determine the reaction time of selenium (+4) precipitation.

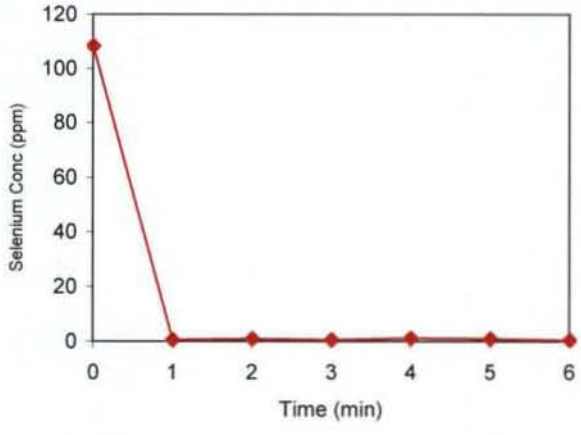


**Figure 19 – The concentration profile of selenium (+4) during the reaction**

The results show that the reduction of selenites ($Se^{4+}$) is extremely fast. Selenium is reduced to below 1 ppm (more than 99% conversion) in less than one minute. The results are in agreement with the findings by Weir et al. (1982) where the reduction reaction was

complete in less than sixty seconds. The precipitate was black in colour signifying copper selenide (Clark, 1975; Hofirek, 1981; Weir et al. 1982). XRD analysis results (Figure 20) also confirmed that the precipitate was indeed copper selenide as depicted by the matching of sample peaks to the reference peaks ($Cu_2Se$).

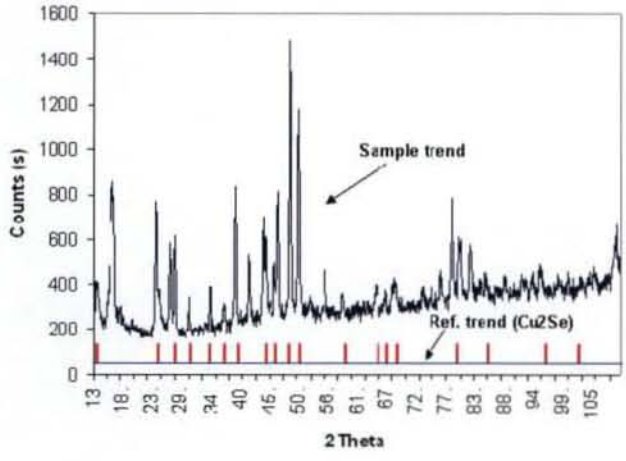


**Figure 20 – XRD analysis of one of the solid samples**

Figure 21 shows the results of the batch experiments to determine the rate of selenium (+6) precipitation from the copper sulphate solution with the error bars indicating the error associated with the analysis using ICP-MS.

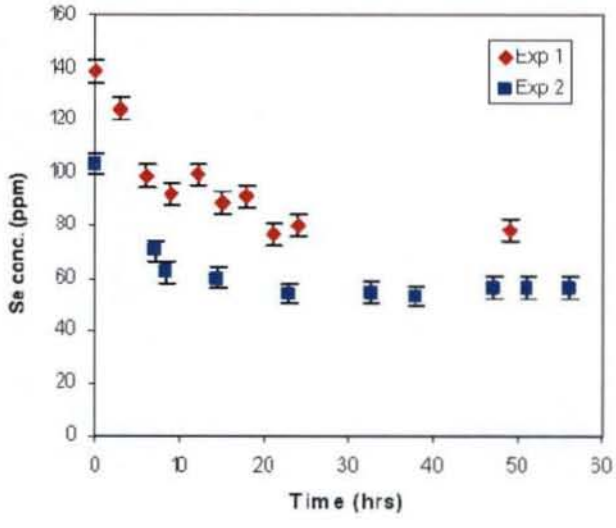


**Figure 21 – Reduction of selenium (+6) using sodium sulphite**

The results show that the reduction of selenium (6+) ions from solution is extremely slow. From the graph, a conversion of only 45.7% is achieved in 72 hours for experiment 2 with the initial concentration being 101ppm while 44.0% conversion is achieved for a slightly higher concentration (138ppm) in experiment 1. The results show consistence in the slow nature of the reduction of the +6 selenium species. If the above results are extrapolated to 99% conversion, the reduction would take an infinite amount of time. This slow reduction is in confirmation with previous studies on the reduction of the selenate species using different reductants (Maiers, 1988; Sharmasarkar and Vance, 2002; Hofirek, 1981).

A reddish-brownish precipitate was also deposited on the walls of the jacketed glass reactor. This precipitate was copper which precipitated according to the disproportionation reaction. It is therefore evident that the cuprous ions that are crucial for the precipitation of selenium are also depleted by this side reaction and hence the need to add sodium sulphite in excess is justified. Hofirek (1981) also observed the same phenomenon and proposed that the cuprous ion can be stabilised by operating at a higher temperature (140-150°C). Figure 22 shows the results of the batch experiment to determine the rate of selenium reduction if both species (+6 and +4) are in solution and also to investigate if selenium (+4) has any catalytic effect on selenium (+6) reduction. The error bars describe the error associated with the actual analysis of the sample using ICP-MS.

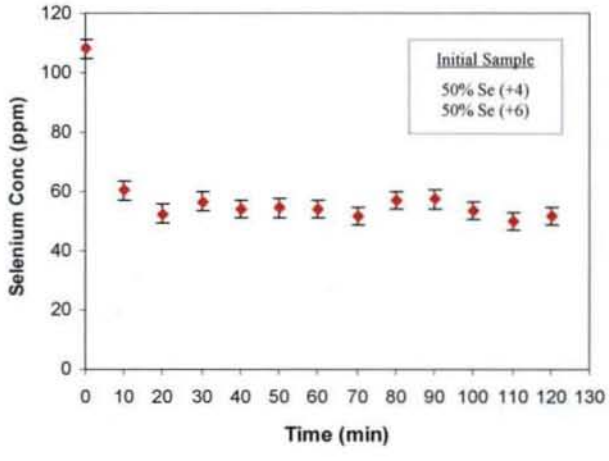


**Figure 22 – The concentration profile of mixed valence selenium during the reaction**

The results show that there is an initial rapid reduction of selenium in the first ten minutes (about 52% conversion). Thereafter, there was no further significant selenium reduction. The initial rapid drop is probably due to Se (+4) reduction precipitation which constituted 50% of the selenium in solution. The above results are not in agreement with Weir et al. (1982) who concluded that the presence of $Se^{4+}$ in solution catalyses the removal of $Se^{6+}$. A possible explanation for this is that the behavior of these species under a higher pressure (10 bar) as studied by Weir et al. (1982) is different than at a lower pressure (1 bar).

The precipitates from the three case studies (100% $Se^{4+}$, 100% $Se^{6+}$ and 50% of both) were analysed using the Scanning Electron Microscope in order to shed light on their nature. The results are displayed in Figure 23.

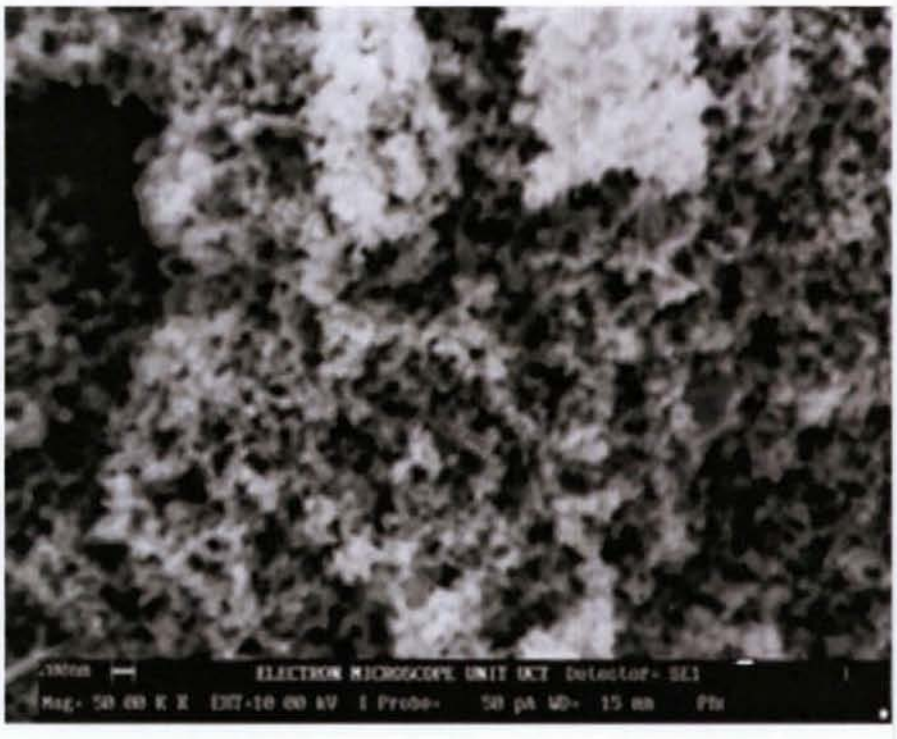

23(a)

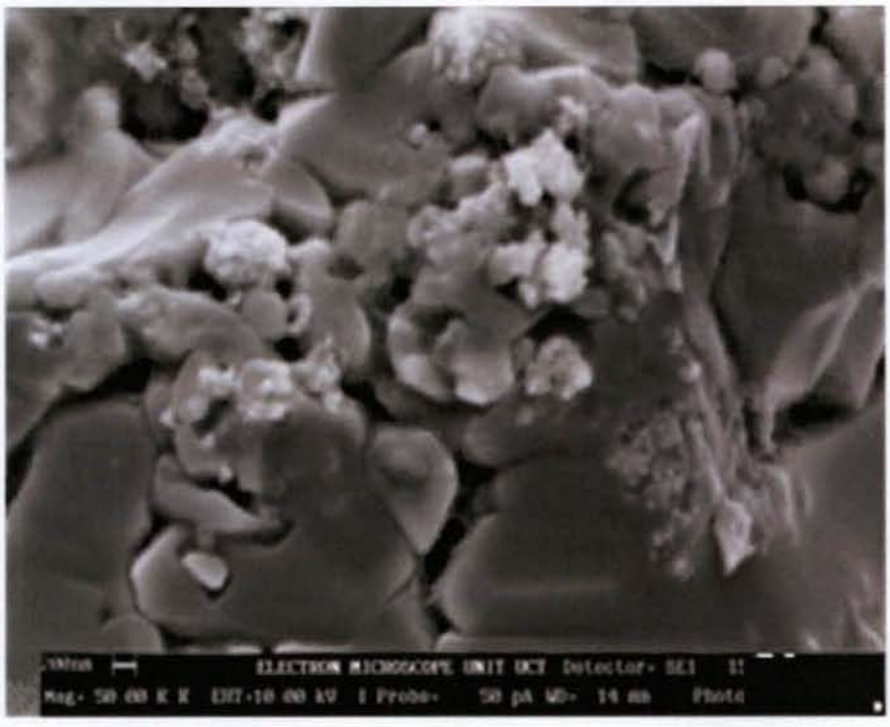

23(b)

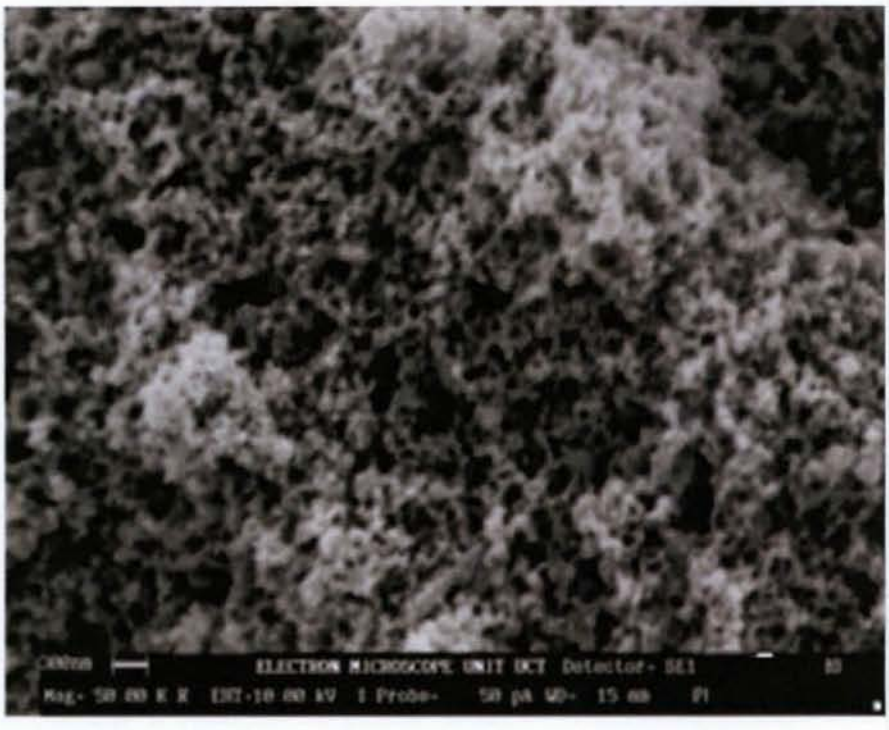

23(c)

**Figure 23 – Se (+4) reduction (23a), Se (6+) reduction (23b) and reduction of equimolar selenium species (23c)**

The results reveal that in both 23(a) and 23(c), more copper selenide (seen by the many very small particles in picture) is produced while during $Se^{6+}$ reduction (23b), there is more element copper precipitated (seen by large smooth particles) than in the other experiments. This is because in the absence of any selenide ions ($Se^{6+}$ reduction is slow), most of the cuprous ions ($Cu^{+}$) undergo disproportionation.

It was noted that on addition of the sodium sulphite into the reactor there were colour changes from the blue colour of copper sulphate to a greenish-blue colour followed by a greenish yellow colour and eventually the reactor contents returned to a blue colour. These colour changes signified formation of intermediate complexes during the reaction. It was hypothesized that these complexes resulting in the colour changes were those between copper and sulphur.

### 4.3 Significance of copper interactions with sulphite ions

Experimental observations showed that a yellowish-brown precipitate was formed immediately on addition of sodium sulphite. In the first experiment, the suspension rapidly dissolved, yielding a light green solution. However, in the second experiment (with excess sodium sulphite), the solution went on to take a yellowish colour which rapidly diminished to a colorless solution. In both experiments, as the precipitate dissolved, a brick red precipitate began to sediment at the bottom of the test tube. This precipitate was more prevalent in the second experiment than the first one due to the excess sodium sulphite used. This precipitate rapidly dissolved on addition of excess sulphuric acid.

The precipitate formed was analysed using Scanning Electron Microscopy (SEM) and Energy Dispersive Spectroscopy (EDS) in order to identify its constituents. The results are displayed in Figure 24 and Figure 25.

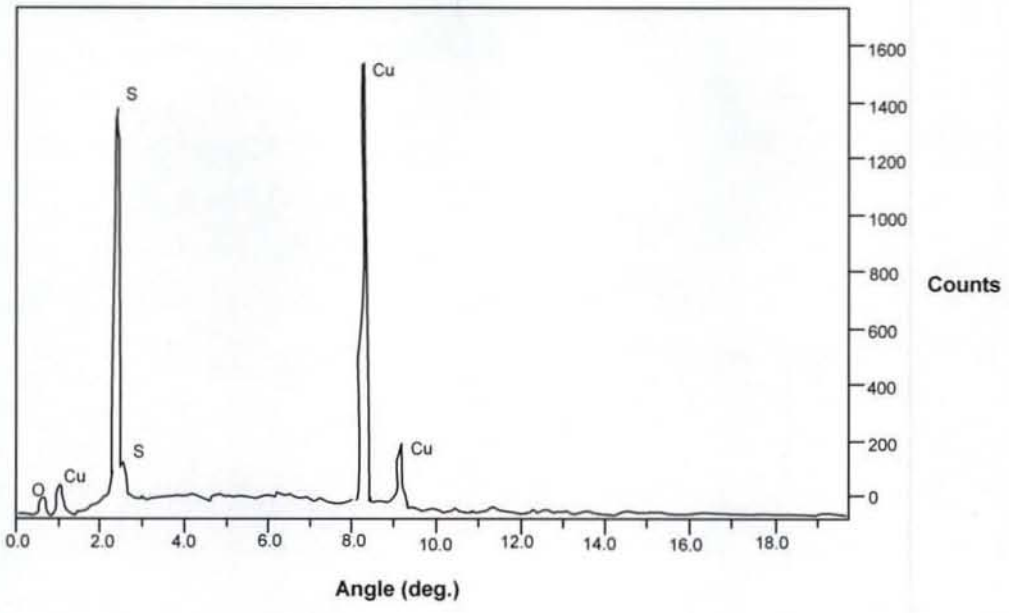


**Figure 24 – Energy dispersion spectroscopy analysis of the precipitate.**


**Figure 25 – Scanning Electron Microscopy photograph of reaction precipitate.**

The EDS results show that the intermediate compound formed contains copper, sulphur and oxygen. The most likely sulphur bearing compound is a mixed valence copper sulphite, $Cu_2SO_3.CuSO_3.2H_2O$ (Chevreul's salt). The SEM picture (Figure 25) showed irregular shaped crystals of the complex signifying its instability as it slowly dissolved when the sample was being prepared. Further EDS analysis carried out to determine the ratio of these elements in the precipitate revealed that copper was in excess of its

constituency in the sulphur bearing compound (Table 3). This would suggest the existence of another complex (most likely $CuSO_3$) or element copper.

**Table 3 – Constituents of precipitate as a percentage**

| Element | Weight (%) | Atomic (%) |
|---|---|---|
| Oxygen (O) | 1.52 | 4.93 |
| Sulphur (S) | 17.78 | 28.89 |
| Copper (Cu) | 80.7 | 66.17 |

From the results, it is apparent that the colour changes that take place in the precipitation process are from the redox reactions involving copper and the sulphur bearing sulphite ions. The yellowish brownish colour can be attributed to the cupric ion - sulphite complex which is formed instantly on mixing according to equation 27. The cupric sulphite complex intermediate formed is very unstable and a rapid reduction of the cupric ion to cuprous ion ($Cu^+$) takes place with the sulphite being oxidized to the sulphate ion according to equation 28. The cuprous ion (Cu+) will then react with available selenide ions to precipitate copper selenide. However in the absence of the selenide ions, especially in Se(+6) reduction, the cuprous ions are reduced to element copper before reacting with selenide ions.

## 4.4 Molecular modeling

In order to explain the differences in the reactivity of selenites and selenates, a theoretical study of the molecular structures of the selenite ($SeO_3^{2-}$), free selenate ion ($SeO_4^{2-}$) and the protonated selenate ion ($HSeO_4^{2-}$) was carried out. This is because the initial molecular structures of the reactants have a significant bearing on the reaction rate and mechanism. Figures 26(a), 26(b) and 26(c) show the structures of selenite, free selenate and protonated selenate respectively.

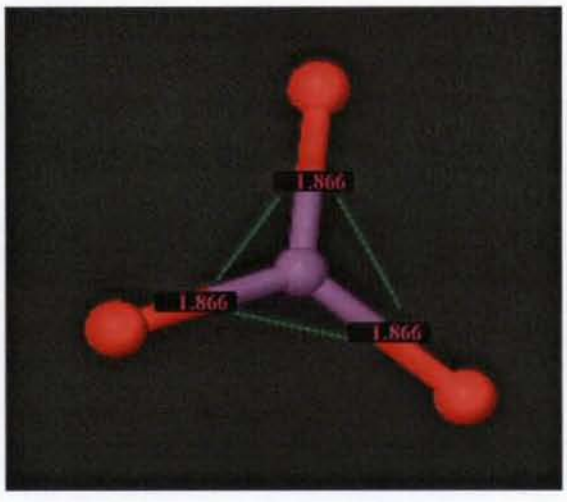


(a)

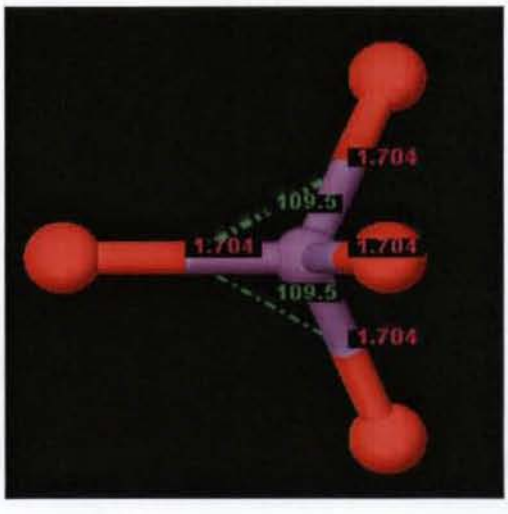


(b)

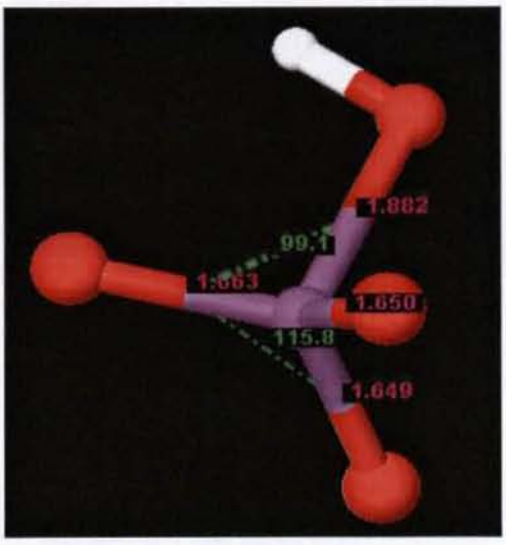


(c)


**Figure 26 – (a) Structure of a selenite ($SeO_3^{2-}$) ion; (b) Structure of a free selenate ($SeO_4^{2-}$) ion; (c) Structure of protonated selenate ion ($HSeO_4^{2-}$)**

The selenite ion 26(a) has a trigonal planar structure with equal bond lengths and bond angles. Figure 26(b) shows that the free selenate ion has a tetrahedral molecular symmetry. The S-O bond lengths are exactly the same at 1.704Å while all the O-S-O bond angles are 109.5°. Dipole moment calculations showed that the ion possesses zero dipole moments. These features make the structure rigid and very unreactive despite the fact that there is a high electron density with a high oxidation state of (+6). In summary, the S-O bonds are difficult to rupture to initiate the reduction reaction.

Figure 26 (c) shows that protonation of the free selenate ion alters both the molecular structure and the electron distribution. Results show that the S-OH bond is elongated to 1.882Å while the S-O bonds are shortened to 1.649Å. Dipole moment calculation results showed that this ion possesses a dipole moment of 1.847 Debye. Hence the protonated selenate ion is more polarized than the free selenate ion. The elongated S-OH bond and the high polarity of the ion are the weak points which make bond breakage easier for the protonated ion than in the free selenate ion. These results are in agreement with

experimental results which showed that selenate reduction is faster in an acidified environment as a result of the protonation of the free selenate ions.

After comparison of the individual reacting molecules, a theoretical investigation of the interaction of the free selenite, free selenate and hydrogen selenate ions with the sulphite ion was carried out. The molecular geometry of the reactants was fully optimized (equilibrium geometry calculation). Vibrational frequencies for the optimized reactants displayed zero imaginary frequencies. Hence these were identified as local minima. The transition state search was carried out using the standard method. The molecular structures of the transition states were also fully optimized and positively identified as saddle points (only one imaginary frequency appeared). Figure 27 shows transition state structures for the free selenite (27a), free selenate (27b) and hydrogen selenate (27c) reduction reactions with sulphite ions.

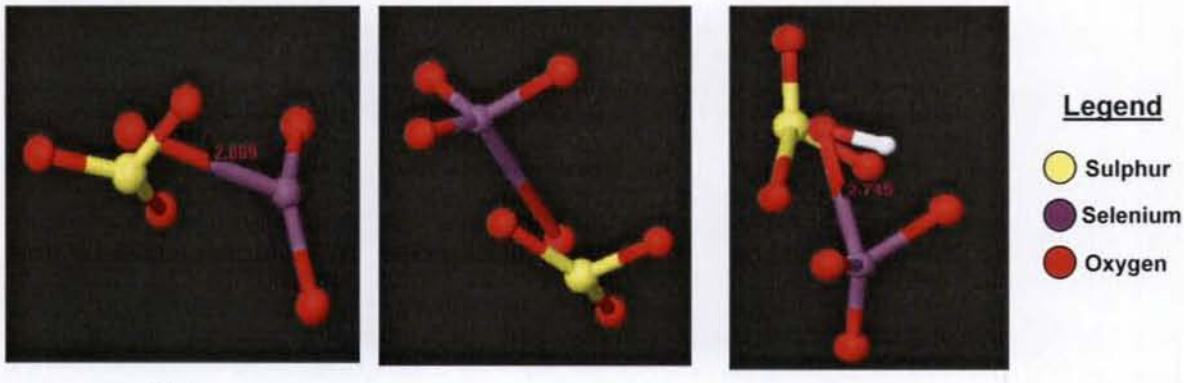


*2(a)* *2(b)* *2(c)*

**Figure 27 – Transition state structures for the free selenite (a), free selenate (b) and hydrogen selenate (c)**

It can be observed from Figure 27 that one of the S-O bonds has stretched; from 1.704 Å to 2.809 Å in the selenite, from 1.704 Å to 1.869 Å in the free selenate and from 1.704 Å to 2.745 Å in the protonated selenate transition states. The elongated bonds in the transition states are the ones that will rupture during the reduction reaction, with the sulphite ion being oxidized to $SO_4^{2-}$. The S-O bond elongation is much longer in the selenite transition state (2.809 Å) than in the protonated selenate (2.745 Å) and the free selenate (1.869 Å).

However, in the free selenate, the oxygen is strongly held as it is closer to the selenium nucleus hence it is envisaged that its reduction is slow. It can also be observed that protonation of the free selenite changes its reactivity. Figure 27c shows that the S-OH bond length in the protonated species is much longer than the S-O in the free selenate.

Table 4, 5 and 6 shows the calculated energies for the selenate reduction reaction using a sulphite based reductant. Solvation energy ($E_{sol}$) was calculated by including solvation effects using the continuum-solvation technique with the Poisson–Boltzmann (PB) approach.

From the calculated results, the reduction step of the free selenate has the highest activation energy of 4.354 kcal/mol (18.217 kJ/mol). Protonation of the free selenate reduces the activation energy to 3.914 kcal/mol (16.38kJ/mol). The activation energy for the selenite species is 3.054 kcal/mol (12.78 kJ/mol). This indicates a very small difference (0.86 kcal/mol) in the activation energies of the selenite and the selenate species. Such a small difference in the activation energies does not completely correlate to experimental results which showed that the reduction of selenite is much faster than that predicted by the difference in activation energies.

**Table 4 – Calculated energies for the free selenite ion ($SeO_3^{2-}$) and sulphite ion interaction**

| Configuration | $E_0$ | | ZPE | S (T=95°C) | | H(T=95°C) | G(T=95°C) | $E_{sol}$ | ΔG |
|---|---|---|---|---|---|---|---|---|---|
| | Hartree | kcal/mol | kcal/mol | cal/mol.K | kcal/mol | kcal/mol | kcal/mol | kcal/mol | kcal/mol |
| $SeO_3^{2-}$ - $SO_3^{2-}$ (R) | -858.493 | -538712.593 | 11.965 | 107.159 | 39.455 | 8.840 | -30.615 | -211.220 | -538942.463 |
| $SeO_3^{2-}$ - $SO_3^{2-}$ (TS) | -858.482 | -538705.796 | 11.680 | 103.510 | 38.111 | 8.308 | -29.803 | -215.490 | -538939.409 |
| Difference | 0.011 | 6.797 | -0.285 | -3.649 | -1.344 | -0.532 | 0.812 | -4.270 | 3.054 |

**Table 5 – Calculated energies for the free selenate ion ($SeO_4^{2-}$) and sulphite ion interaction**

| Configuration | $E_0$ | | ZPE | S (T=95°C) | | H(T=95°C) | G(T=95°C) | $E_{sol}$ | ΔG |
|---|---|---|---|---|---|---|---|---|---|
| | Hartree | kcal/mol | kcal/mol | cal/mol.K | kcal/mol | kcal/mol | kcal/mol | kcal/mol | kcal/mol |
| $SeO_4^{2-}$ - $SO_3^{2-}$ (R) | -933.631 | -585862.126 | 13.901 | 113.114 | 41.647 | 9.689 | -31.959 | -198.980 | -586079.163 |
| $SeO_4^{2-}$ - $SO_3^{2-}$ (TS) | -933.624 | -585857.722 | 13.719 | 106.368 | 39.164 | 9.058 | -30.106 | -200.700 | -586074.809 |
| Difference | 0.007 | 4.403 | -0.182 | -6.746 | -2.484 | -0.631 | 1.853 | -1.720 | 4.354 |

**Table 6 – Calculated energies for the hydrogen selenate ion ($HSeO_3^-$) and sulphite ion interaction**

| Configuration | $E_0$ | | ZPE | S (T=95°C) | | H(T=95°C) | G(T=95°C) | $E_{sol}$ | ΔG |
|---|---|---|---|---|---|---|---|---|---|
| | Hartree | kcal/mol | kcal/mol | cal/mol.K | kcal/mol | kcal/mol | kcal/mol | kcal/mol | kcal/mol |
| $HSeO_4^{2-}$ - $SO_3^{2-}$ (R) | -934.348 | -586312.11 | 21.593 | 119.818 | 44.116 | 10.351 | -33.765 | -57.500 | -586381.783 |
| $HSeO_4^{2-}$ - $SO_3^{2-}$ (TS) | -934.344 | -586309.547 | 21.362 | 111.297 | 40.978 | 9.554 | -31.424 | -58.260 | -586377.869 |
| Difference | 0.004 | 2.565 | -0.231 | -8.521 | -3.137 | -0.797 | 2.341 | -0.760 | 3.914 |

## 4.5 Nucleation kinetics

Figures 28 to 31 show the results of the number of particles ($N_p$) versus residence time plot for the four supersaturation ratios.

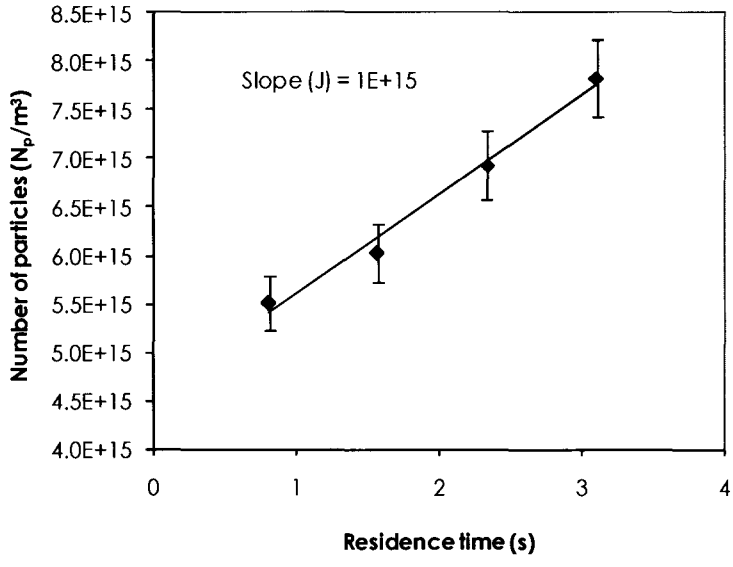


**Figure 28 – Supersaturation of $8.66x10^{15}$ yielding a nucleation rate J = $1.0x10^{15}$ $m^{-3}s^{-1}$**

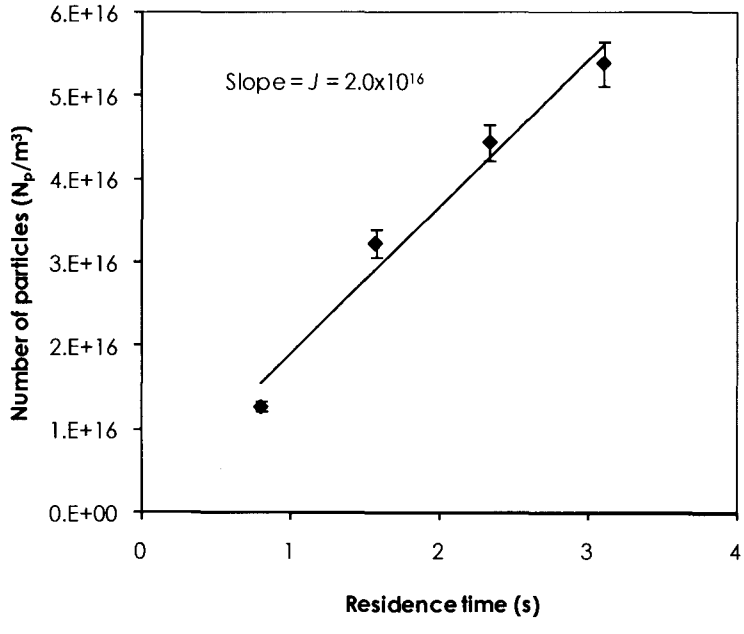


**Figure 29 – Supersaturation of $2.17x10^{16}$ yielding a nucleation rate J = $2.0x10^{16}$ $m^{-3}s^{-1}$**

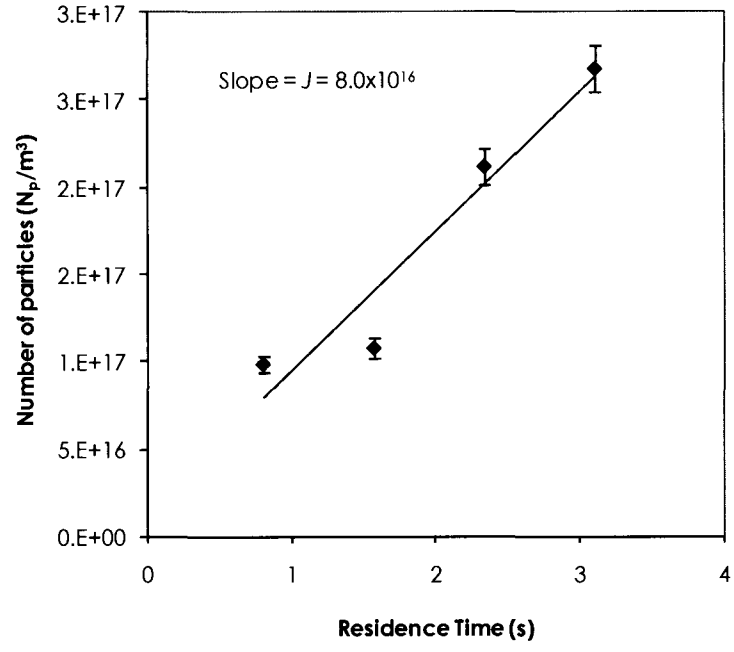


**Figure 30 – Supersaturation of $4.32x10^{16}$ yielding a nucleation rate J = $8.0x10^{16}$ $m^{-3}s^{-1}$**

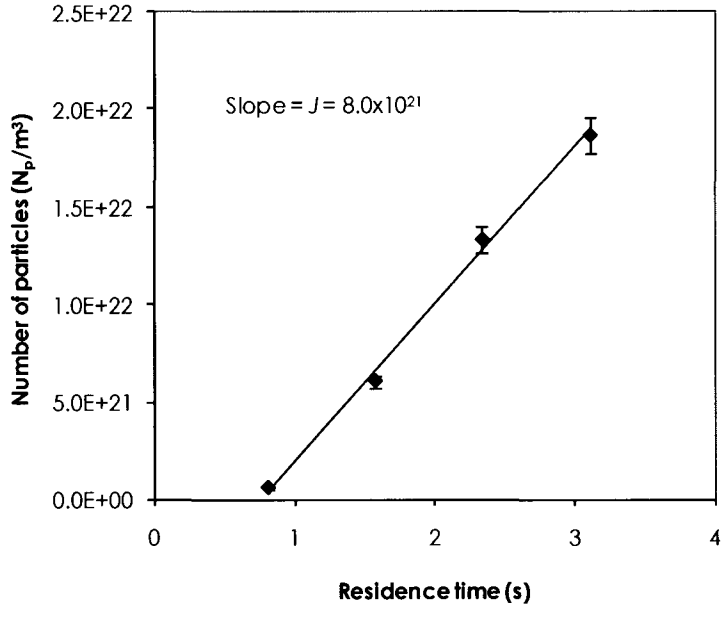


**Figure 31 – Supersaturation of $4.33x10^{17}$ yielding a nucleation rate J = $8.0x10^{21}$ $m^{-3}s^{-1}$**

From the graphs, it can be observed that there is an increase in the number of particles with increasing residence time. This behavior is expected if equation 13 holds, as an increased residence time allows greater contact time for more particles to nucleate. The nucleation

rate was calculated for the four supersaturation levels according to equation 14. The results are shown in Table 7.

**Table 7 – Nucleation rates for the investigated supersaturations**

| Supersaturation ratio (S) | Nucleation rate (J) ($m^{-3}s^{-1}$) |
|---|---|
| $8.66x10^{15}$ | $1.0x10^{15}$ |
| $2.17x10^{16}$ | $2.0x10^{16}$ |
| $4.32x10^{16}$ | $8.0x10^{16}$ |
| $4.33x10^{17}$ | $8.0x10^{21}$ |

It can also be observed that the nucleation rate increases gradually with an increase in supersaturation level. This trend is consistent with previous studies (Kashchiev and Rosmalen, 2003; Roelands et al. 2005) on different precipitation systems which showed that nucleation rate increases with increasing levels of supersaturation. In order to derive more useful information for this precipitation system, the natural logarithm of the supersaturation to nucleation rate ratio (ln(J/S)) was plotted against $1/(\ln^2 S)$ according to equation 6. The plot is shown in Figure 32.

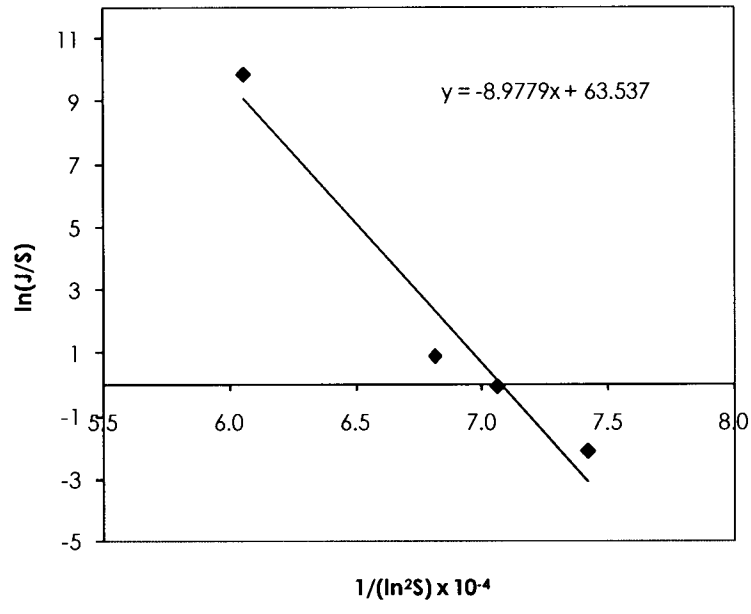


**Figure 32 - The natural logarithm of the supersaturation to nucleation rate ratio (ln (J/S)) against $1/(\ln^2 S)$ graph**

According to equation 6, the intercept of the graph determines the kinetic parameter *A* while the gradient gives thermodynamic constant *B*. The calculated results showed that; $A=3.92x10^{27}$ $m^{-3}s^{-1}$ and $B=8.98x10^{04}$. The thermodynamic parameter (*B*) was used to compute the nucleation work (*W**) and the critical nucleus size (*n**) according to equations 7 and 8 respectively. The calculated values of these parameters for the four different supersaturation ratios are displayed in Table 8.

**Table 8 – Calculated values of nucleation work and nucleus size**

| Supersaturation ratio (S) | Nucleus size (n*) | Nucleation work ($W^*/_{kT}$) |
|---|---|---|
| $8.66x10^{15}$ | 3.63 | 66.66 |
| $2.17x10^{16}$ | 3.37 | 63.44 |
| $4.32x10^{16}$ | 3.19 | 61.19 |
| $4.33x10^{17}$ | 2.68 | 54.44 |

From Table 7, it can be deduced that the nucleus size decreases with an increase in supersaturation. This is in line with previous studies and theory (Sohnel and Garside, 1992). For the supersaturation levels investigated, the results show that the critical nucleus size (n*) is very small, consisting of between 2 to 4 particles. This result is consistent with SEM images and measurements using the dynamic light scattering (DLS) technique which showed that the particles are in the nano range. Such a small size of the critical nucleus size also confirms why the particles instantaneously appear upon contact of the reagents. The results also show that the energy barrier to nucleation (nucleation work) decreases with an increase in supersaturation and that the nucleation energy for this system is extremely small. Again, this is consistent with the precipitation system under consideration because it involves high supersaturation levels.

The kinetic constant *A* ($3.92x10^{27}$ $m^{-3}s^{-1}$) is relatively high and according to Kashchiev and van Rosmalen (2003), this is an indication of a homogeneous nucleation dominated system. Since the experiments were carried out under high supersaturation levels, such a high value of A is expected. The high value of the kinetic parameter is due to a high frequency of monomer attachment to the nuclei. Therefore this confirms that seeding has an insignificant effect on the nucleation kinetics of selenium precipitation.

The instantaneous formation of the critical nucleus size shows that the nucleation process is not the rate limiting step in selenium precipitation. It is therefore predicted that the rate limiting step is the chemical reaction rather than the particle formation processes.

The particles formed are very small, which may lead to filtration problems. Hence other secondary processes like aggregation and Oswald ripening must be promoted to increase particle size, thereby improving filterability. This could be done by setting an optimum agitation rate and a longer contact time. Growth is minimal due to the high supersaturation levels and their rapid consumption.

## 5.0 CONCLUSIONS

I. Reduction of selenium from copper sulphate solution needs to be carried out under acidic conditions (pH<3) in order to prevent copper co-precipitating as oxides. Reduction of selenites (Se+4) is extremely fast with a 99.9% conversion being achieved in less than 60 seconds. However, un-catalyzed reduction of selenate (+6 oxidation state) is extremely slow with a 45.77% conversion being achieved in seventy two hours.

II. Selenate is difficult to reduce due to its rigid structure which has a zero dipole moment. The activation energies of selenite, free selenate and hydrogen selenate interaction with sulphite ions show a trend that is in agreement with experimental evidence i.e. rate of reaction of selenite>hydrogen selenate>free selenate.

III. It is therefore not practical to develop a continuous selenium precipitation process due to the long residence time required for the +6 oxidation state to be reduced to the required levels. An ion that will form a more reactive complex with selenate (+6 oxidation state) is required to shorten the reaction time. It is suggested that such an ion can be searched for using the molecular modeling approach. The desired ion should significantly reduce the activation energy of the selenate/sulphite ion interaction reaction to that similar to selenite reduction.

IV. It can also be concluded that selenite does not have any significant catalytic effect on selenate reduction. Therefore its presence in solution does not reduce the selenate reaction time.

V. Element copper and a mixed valence copper – sulphite salt called Chevreul's salt ($Cu_2SO_3.CuSO_3.2H_2O$) may be precipitated together with copper selenide during the selenium precipitation process (if the solution pH is above 2.0 for Chevreul's salt). More copper is precipitated if the solution is abundant in selenate. Because of these side reactions, sodium sulphite needs to be added in excess.

VI. The kinetic parameter ($A$) for the selenium precipitation process was estimated to be $3.92 \times 10^{27}$ $m^{-3}s^{-1}$ and the thermodynamic constant ($B$) was calculated to be $8.98 \times 10^{04}$. Therefore the relationship between nucleation rate ($J_s$) and supersaturation ratio ($S$) for selenium precipitation is given by:

$$J_s = 3.92x10^{27}(S)exp\left[\frac{-8.98x10^{04}}{ln^2 S}\right] \quad [29]$$

VII. The nucleation work in selenium precipitation is very small. As a result nucleation is spontaneous and takes place through a homogenous mechanism. Therefore seeding is of less importance in this process.

VIII. The critical nucleus of copper selenide is very small (between 2 and 4 particles). This may lead to filtration problems hence an aging process needs to be promoted to increase the particle size thereby significantly improving filterability.

## 6.0 RECOMMENDATIONS

In order to develop a continuous selenium precipitation process, there is need to significantly reduce the reaction time for the reduction of $Se^{+6}$ to $Se^{+4}$. Therefore studies should focus on finding possible ways to speed up the reduction reaction of selenium (+6) to selenium (+4) oxidation state. The investigation process can be achieved through (i) trying different reagents in a series of experiments to determine the desired reductant (one that will results in a faster reduction), (ii) trying different possible catalysts with sulphur based reagents as reductants, (iii) finding an ion that can destabilize the selenate structure to make it more reactive and (iv) carrying out the experiment under high temperature and pressure. Based on previous studies (Hofirek, 1981) a temperature of 175°C and pressure of 10 bar is recommended as a starting point. These aspects can be investigated experimentally or can be carried out theoretically using commercial modeling programs like Jaguar 7.5 (Schrodinger, Inc., Portland, OR) for aqueous systems.

Since selenium and tellurium are both impurities in the copper electrowinning solution, further studies can also be carried out to investigate the reduction kinetics of tellurium. However the reduction chemistry of tellurium is expected to be similar to that of selenium due their proximity within group 6 of the periodic table.

## 7.0 REFERENCES


Asperger, S. (ed) 2003, *Chemical Kinetics and Inorganic Reaction Mechanisms*, 2nd edn, Kluwer Academic/Plenum Publishers, New York.

Blandin, A.F., Mangin, D., Nallet, V., Klein, J.P. & Bossoutrot, J.M. 2001, "Kinetics identification of salicylic acid precipitation through experiments in a batch stirred vessel and a T-mixer", *Chemical Engineering Journal,* vol. 81, no. 1-3, pp. 91-100.

Brimmer, S.P., Fawcett, W.R. & Kulhavy, K.A. 1987, "Quantitative reduction of selenate ion to selenite in aqueous samples", *Anal. Chem.,* vol. 59, no. 10, pp. 1470-1471.

Calban, T., Colak, S. and Yesilyurt, M. 2006, "Statistical modeling of Chevreul's salt recovery from leach solutions containing copper", *Chemical Engineering and Processing,* vol. 45, pp. 168-174.

Clark, F.F. & Rickard, R.S. 1975, *Method of removing selenium from copper sulphate solution*, United States Patent 3,914,375.

Conklin, M.H. & Hoffmann, M.R. 1988, "Metal ion - sulfur (IV) chemistry. 2. Kinetic studies of the redox chemistry of copper II - sulphur (IV) complexes", *Environmental Engineering Science,* vol. 22, no. 8, pp. 891-898.

Elrashidi, M.A., Adriano, D.C. & Lindsay, W.L. 1989, "Solubility, speciation and transformations of selenium in soils", *Selenium in agriculture and the environment,* vol. 23, pp. 51-63.

Elrashidi, M.A., Adriano, D.C., Workman, S.M. & Lindsay, W.L. 1987, "Chemical equilibria of selenium in soils: A theoretical development", *Soil Science,* vol. 144, no. 2, pp. 141-152.

Fujita, M., Ike, M., Hashimoto, R., Nakagawa, T., Yamaguchi, K. & Soda, S.O. 2005, "Characterizing kinetics of transport and transformation of selenium in water–sediment microcosm free from selenium contamination using a simple mathematical model", *Chemosphere,* vol. 58, no. 6, pp. 705-714.

Habashi, F. (ed) 1993, *A text book of Hydrometallurgy*, Metallurgie Extractive Quebec, Enr, Canada.

Hofirek, Z. 1981, *Development of continuous process for selenium removal from sulphate solutions by use of $SO_2$ containing reagents.*, Mattey Rustenburg Refineries, South Africa.

Jackson, E. (ed) 1986, *Hydrometallurgical extraction and reclamation*, Ellis Horwood Limited, England.

Jones, A.G. (ed) 2002, *Crystallisation Process Systems*, Butterworth-Heinemann, Britain.

Kashchiev, D. 2000, *Nucleation: Basic theory with applications,* 1st edn, Butterworth-Heinemann, London.

Kashchiev, D. & van Rosmalen, G.M. 2003, "Review: Nucleation in solutions revisited", *Cryst. Res. Technol,* vol. 38, no. 7-8, pp. 555-574.

Keeler, J. & Wothers, P. (eds) 2003, *Why chemical reactions happen*, 1st edn, Oxford University Press, New York.

Lewis, A & Kramer, H. 2008, "Crystallization Processes", Lecture notes presented to Crystallisation and Precipitation course participants.

Linkson, P.B. 1992, "The stability of selenium in aqueous systems", *Institution of Chemical Engineers,* vol. 70, no. B, pp. 149-152.

Liu, X.Y. 2001, "Interfacial effect of molecules on nucleation kinetics", *J. Phys. Chem.,* vol. 105, pp. 11550-11558.

Lupton, F.S. & Sheridan, W.G. 2008, *System and methods for biological selenium removal from water* , 210/603 edn, C02F3/28, United States of America.

Ma, Q., Ellis, G.S., Amrani, A., Zhang, T. & Tang, Y. 2008, "Theoretical study on the reactivity of sulfate species with hydrocarbons", *Geochimica et Cosmochimica Acta,* vol. 72, pp. 4565-4576.

Mahajan, A.J. & Kirwan, D.J. 1993, "Rapid precipitation of biochemicals", *J. Phys. D: Appl. Phys,* vol. 26, pp. B176-B180.

Maiers, D.T., Wichlacz, P.L., Thompson, D.L. & Bruhn, D.F. 1988, "Selenate reduction by bacteria from a selenium-rich environment", *Applied and Environmental Microbiology,* vol. 54, no. 10, pp. 2591-2593.

Maneval, J.E., Klein, G. & Sinkovic, J. 1985, *Selenium removal from drinking water by ion exchange*, Water Engineering Research Laboratory, Cincinnati.

McGrew, K. J., Murphy, J. & Williams, D. "Selenium Reduction via Conventional Water Treatment," Randol Gold Forum 1996, (Denver, CO, Randol Gold Int., 1996), pp 129-41.

Merrill, D.T., Manzione, M.A., Parker, D.S., Petersen, J.J., Chow, W. & Hobbs, A.O. 1987, "Field evaluation of arsenic and selenium removal by iron coprecipitation", *Environmental Progress,* vol. 6, no. 2, pp. 82-90.

Mersmann, A. (ed) 2001, *Crystallisation Technology Handbook*, 2nd edn, Marcel Dekker Inc., New York.

Mohan, R. & Myerson, A.S. 2002, "Growth kinetics: A thermodynamic approach", *Chemical Engineering Science,* vol. 57, no. 20, pp. 4277-4285.

Mortimer, M. & Taylor, P. (eds) 2002, *The Molecular World*, 2nd edn, Royal Society of Chemistry, UK.

Mullin, J.W. (ed) 1972, *Crystallisation*, 2nd Edition edn, Butterworth and Co. Ltd, London.

Murphy, A.P., "Removal of Selenate from Water by Chemical Reduction," Industrial and Engineering Chemical Research, Vol. 27, pp.187-191, 1988

Myerson, A.S. (ed) 2002, *Handbook of Industrial Crystallisation*, 2nd Edition edn, Butterworth Heinemann, United States of America.

Nielsen A.E.1979 ,'Industrial crystalisation' ,Amsterdam:Jong and Jancic

Nikolic, C.B. & Laferty, J.M. 1981, *Precipitation of selenium from copper electrowinning solutions*, Canadian Patent 1,1134.

OLI systems Inc Stream Analyser, 2004. Version 2.0.57, OLI Systems Inc, Morris Plains, New Jersey.

Outokumpu Research Oy. 2002, Pori, Finland, A. Roine.

Polanyi, D.C. (ed) 1972, *Chemical Kinetics*, Butterworth, London.

Rafal, M., Berthold, J. & Linz, D. 2001, *Introduction to OLI Electrolytes*, OLI sytsems Inc., New Jersey.

Richardson, C.B. & Snyder, T.D. 1994, "A study of heterogenous nucleation in aqueous solutions", *Langmuir,* vol. 10, pp. 2462-2465.

Roelands, C.P.M. 2005, *Polymorphism in precipitation processes*, Delft University of Technology, Netherlands.

Schrödinger, Inc. Jaguar 7.0.109, 1500 SW First Avenue, Suite 1180, Portland, OR 97201. www.schrodinger.com

Schubert, H. & Mersmann, A. 1996, "Determination of heterogeneous nucleation rates", *Trans IChemE,* vol. 74, no. Part A, pp. 821-827.

Séby, F., Potin Gautier, M., Lespés, G. & Astruc, M. 1997, "Selenium speciation in soils after alkaline extraction", *Science of The Total Environment,* vol. 207, no. 2-3, pp. 81-90.

Séby, F., Potin-Gautier, M., Giffaut, E., Borge, G. & Donard, O.F.X. 2001, "A critical review of thermodynamic data for selenium species at 25°C", *Chemical Geology,* vol. 171, no. 3-4, pp. 173-194.

Sharmasarkar, S., Reddy, K.J. & Vance, G.F. 1996, "Preliminary quantification of metal selenite solubility in aqueous solutions", *Chemical Geology,* vol. 132, no. 1-4, pp. 165-170.

Sharmasarkar, S. & Vance, G.F. 2002, "Soil and plant selenium at a reclaimed uranium mine", *J. Environ. Qual.,* vol. 31, no. 31, pp. 1516-1521.

Sohnel, G. & Garside, J. 1992, *Precipitation:Basic Principles and Applications,* Butterworth-Heinemann, UK.

Sorg, T.J. & Logsdon, G.S. 1978, "Treatment Technology to meet interim primary drinking water regulations for inorganics:Part 2", *J. AWWA,* , pp. 379-393.

Tan, T.Y.T. 2003, *Photocatalytic reduction of selenate and selenite:Water/Waste water treatment and the formation of Nano-selenium compounds.*, The School of Chemical Engineering and Industrial Chemistry: The University Of New South Wales.

Trussell, R.R., Trussell, A. & Kreft, P. (eds) 1980, *Selenium removal from ground water using activated alumina*, Municipal Environmental Research Laboratory, Cincinnati, Springfield, Va.

Twidwell, L.G., J. McCloskey, P. Miranda, and M. Gale. 1999. Potential technologies for removing selenium from process and mine wastewater. p 1645-1656. Proceeding REWAS-99. San Sebastian. Spain. September 5-9.

Qin-bo, W., Finsy, R., Hai-bo, X., and Xi, L. 2005. On the critical radius in generalized Ostwald ripening. Journal of Zhejiang University Science, vol. 8, pp 705-707.

Weir, D.R., Kerfoot, D.G.E. & Scheie, H.C. 1982, *Removal of selenium (IV) and (VI) from acidic copper sulphate solutions*, United States Patent 4,330,508.

Wojciechowski, B.W. & Rice, N.M. (eds) 2003, *Experimental Methods in Kinetic Studies*, 2nd edn, Elsevier, Netherlands.

Zingaro, R.A. & Cooper, W.C. (eds) 1974, *Selenium*, 1st edn, Van Nostrand Reinhold Company, New York.

Zingaro, R.A., Dufner, D.C., Murphy, A.P. & Moody, C.D. 1997, "Reduction of oxoselenium anions by iron II hydroxide", *Environment International,* vol. 23, no. 3, pp. 299-304.

# APPENDICES

## Appendix A

Species in the initial copper sulphate solution at 95°C and 1 atmosphere (Modeled using OLI Stream Analyzer 2.0)

| Species Output (True Species) | Total (mol) | Aqueous (mol) | Vapor (mol) | Solid (mol) |
|---|---|---|---|---|
| $H_2O$ | 55.5087 | 55.5087 | 0 | 0 |
| $H_2SO_4$ | 9.84E-14 | 9.84E-14 | 0 | 0 |
| $Cu(OH)_2$ | 4.93E-10 | 4.93E-10 | 0 | 0 |
| $H_2$ | 1.49E-32 | 1.49E-32 | 0 | 0 |
| $H_2SeO_3$ | 8.14E-04 | 8.14E-04 | 0 | 0 |
| $O_2$ | 2.15E-11 | 2.15E-11 | 0 | 0 |
| $SO_3$ | 5.33E-17 | 5.33E-17 | 0 | 0 |
| $Cu(OH)_3^{-1}$ | 7.87E-19 | 7.87E-19 | 0 | 0 |
| $Cu(OH)_4^{-2}$ | 7.56E-27 | 7.56E-27 | 0 | 0 |
| $Cu^{+1}$ | 8.59E-11 | 8.59E-11 | 0 | 0 |
| $Cu^{+2}$ | 1.56998 | 1.56998 | 0 | 0 |
| $CuOH^{+1}$ | 1.88E-05 | 1.88E-05 | 0 | 0 |
| $H^{+1}$ | 0.0197404 | 0.0197404 | 0 | 0 |
| $HSeO_3^{-1}$ | 5.33E-05 | 5.33E-05 | 0 | 0 |
| $HSO_4^{-1}$ | 0.794261 | 0.794261 | 0 | 0 |
| $Na^{+1}$ | 1.07E-03 | 1.07E-03 | 0 | 0 |
| $NaSO_4^{-1}$ | 6.62E-04 | 6.62E-04 | 0 | 0 |
| $OH^{-1}$ | 3.34E-11 | 3.34E-11 | 0 | 0 |
| $SeO_3^{-2}$ | 3.24E-09 | 3.24E-09 | 0 | 0 |
| $SO_4^{-2}$ | 1.18291 | 1.18291 | 0 | 0 |
| Total (by phase) | 59.0782 | 59.0782 | 0 | 0 |

## Appendix B

Species output of selenium precipitation from acidic copper sulphate solution at 95°C and 1 atmosphere (Modeled using OLI Stream Analyzer 2.0)

| Species Output (True Species) | Total (mol) | Aqueous (mol) | Vapor (mol) | Solid (mol) |
|---|---|---|---|---|
| $H_2O$ | 55.4244 | 55.4244 | 0 | 0 |
| $H_2SO_4$ | 1.66E-13 | 1.66E-13 | 0 | 0 |
| $Cu(OH)_2$ | 2.79E-10 | 2.79E-10 | 0 | 0 |
| $Cu_2O$ | 0.0391946 | 0 | 0 | 0.0391946 |
| $Cu_2Se$ | 8.67E-04 | 0 | 0 | 8.67E-04 |
| $H_2$ | 3.92E-16 | 3.92E-16 | 0 | 0 |
| $H_2S$ | 8.56E-22 | 8.56E-22 | 0 | 0 |
| $H_2Se$ | 1.82E-32 | 1.82E-32 | 0 | 0 |
| $H_2SeO_3$ | 2.55E-31 | 2.55E-31 | 0 | 0 |
| $Na_2S_2O_4$ | 7.44E-38 | 7.44E-38 | 0 | 0 |
| $O_2$ | 3.46E-44 | 3.46E-44 | 0 | 0 |
| $SO_2$ | 1.92E-11 | 1.92E-11 | 0 | 0 |
| $SO_3$ | 9.02E-17 | 9.02E-17 | 0 | 0 |
| $Cu(OH)_3^{-1}$ | 3.30E-19 | 3.30E-19 | 0 | 0 |
| $Cu(OH)_4^{-2}$ | 2.23E-27 | 2.23E-27 | 0 | 0 |
| $Cu^{+1}$ | 0.0100519 | 0.0100519 | 0 | 0 |
| $Cu^{+2}$ | 1.47981 | 1.47981 | 0 | 0 |
| $CuOH^{+1}$ | 1.37E-05 | 1.37E-05 | 0 | 0 |
| $H^{+1}$ | 0.0253154 | 0.0253154 | 0 | 0 |
| $HS^{-1}$ | 2.88E-26 | 2.88E-26 | 0 | 0 |
| $HSe^{-1}$ | 3.50E-34 | 3.50E-34 | 0 | 0 |
| $HSeO_3^{-1}$ | 1.23E-32 | 1.23E-32 | 0 | 0 |
| $HSeO_4^{-1}$ | 6.85E-48 | 6.85E-48 | 0 | 0 |
| $HSO_3^{-1}$ | 1.10E-11 | 1.10E-11 | 0 | 0 |
| $HSO_4^{-1}$ | 0.959263 | 0.959263 | 0 | 0 |
| $HSO_5^{-1}$ | 2.01E-37 | 2.01E-37 | 0 | 0 |
| $Na^{+1}$ | 0.0619376 | 0.0619376 | 0 | 0 |
| $NaS_2O_3^{-1}$ | 5.59E-25 | 5.59E-25 | 0 | 0 |
| $NaSO_4^{-1}$ | 0.0351771 | 0.0351771 | 0 | 0 |
| $OH^{-1}$ | 2.54E-11 | 2.54E-11 | 0 | 0 |
| $S^{-2}$ | 1.14E-34 | 1.14E-34 | 0 | 0 |
| $S_2^{-2}$ | 9.67E-46 | 9.67E-46 | 0 | 0 |
| $S_2O_3^{-2}$ | 3.80E-23 | 3.80E-23 | 0 | 0 |
| $S_2O_4^{-2}$ | 6.53E-33 | 6.53E-33 | 0 | 0 |
| $S_2O_5^{-2}$ | 7.55E-27 | 7.55E-27 | 0 | 0 |
| $S_2O_6^{-2}$ | 9.06E-23 | 9.06E-23 | 0 | 0 |
| $S_2O_8^{-2}$ | 1.37E-42 | 1.37E-42 | 0 | 0 |
| $S_4^{-2}$ | 4.14E-69 | 4.14E-69 | 0 | 0 |
| $Se^{-2}$ | 8.35E-45 | 8.35E-45 | 0 | 0 |
| $SeO_3^{-2}$ | 5.27E-37 | 5.27E-37 | 0 | 0 |
| $SeO_4^{-2}$ | 1.43E-47 | 1.43E-47 | 0 | 0 |
| $SO_3^{-2}$ | 1.86E-16 | 1.86E-16 | 0 | 0 |
| $SO_4^{-2}$ | 1.03125 | 1.03125 | 0 | 0 |
| **Total (by phase)** | **59.0673** | **59.0272** | **0** | **0.040062** |